European Journal of Medicinal Chemistry 232 (2022) 114206

Contents lists available at ScienceDirect

European Journal of Medicinal Chemistry

journal homepage: http://www.elsevier.com/locate/ejmech

Discovery of 3*H*-pyrrolo[2,3-*c*]quinolines with activity against *Mycobacterium tuberculosis* by allosteric inhibition of the glutamate-5-kinase enzyme

Michele Panciera [a, b, 1], Emilio Lence [a, 1], Ángela Rodríguez [a], Begoña Gracia [c, d, e], José A. Aínsa [c], Clara Marco-Marín [f], Vicente Rubio [f], Carlos Roque Duarte Correia [b], Concepción González-Bello [a, *]

[a] *Centro Singular de Investigación en Química Biolóxica e Materiais Moleculares (CiQUS), Departamento de Química Orgánica, Universidade de Santiago de Compostela, Jenaro de la Fuente s/n, 15782, Santiago de Compostela, Spain*
[b] *Institute of Chemistry, State University of Campinas, Josue de Castro St, Campinas, São Paulo, 13083-970, Brazil*
[c] *Departamento de Microbiología, Pediatría, Radiología y Salud Pública, Facultad de Medicina and BIFI, Universidad de Zaragoza, Domingo Miral s/n, 50009, Zaragoza, Spain*
[d] *Instituto de Investigación Sanitaria Aragón (IIS-Aragón), Av. San Juan Bosco 13, 50009, Zaragoza, Spain*
[e] *Centro de Investigación Biomédica en Red de Enfermedades Respiratorias (CIBERES), Instituto de Salud Carlos III, Av. Monforte de Lemos 3–5, 28029, Madrid, Spain*
[f] *Instituto de Biomedicina de Valencia (IBV-CSIC), CIBER de Enfermedades Raras (CIBERER-ISCIII), Valencia, Spain*

ARTICLE INFO

Article history:
Received 3 January 2022
Received in revised form
15 February 2022
Accepted 16 February 2022
Available online 22 February 2022

Dedicated to Prof. Joan Bosch on the occasion of his 75th birthday

Keywords:
Allosteric inhibition
Tuberculosis
Target shape-motion
Glutamate-5-kinase
Molecular dynamics simulation studies
Pyrroloquinoline

ABSTRACT

The therapeutic potential of 3*H*-pyrrolo[2,3-*c*]quinolines—the main core of Marinoquinoline natural products—has been explored for the development of new anti-TB agents. The chemical modification of various positions in this scaffold has led to the discovery of two pyrroloquinolines (compounds **50** and **54**) with good *in vitro* activity against virulent strains of *Mycobacterium tuberculosis* (H37Rv, MIC = 4.1 μM and 4.2 μM, respectively). Enzymatic assays showed that both derivatives are inhibitors of glutamate-5-kinase (G5K, encoded by *proB* gene), an essential enzyme for this pathogen involved in the first step of the proline biosynthesis pathway. G5K catalyzes the phosphoryl-transference of the γ-phosphate group of ATP to L-glutamate to provide L-glutamyl-5-phosphate and ADP, and also regulates the synthesis of L-proline. The results of various molecular dynamics simulation studies revealed that the inhibition of G5K would be caused by allosteric interaction of these compounds with the interface between enzyme domains, against different pockets and with distinct recognition patterns. The binding of compound **54** promotes long-distance conformational changes at the L-glutamate binding site that would prevent it from anchoring for catalysis, while compound **50** alters the ATP binding site architecture for recognition. Enzyme assays revealed that compound **50** caused a substancial increase in the K_m^{app} for ATP, while no significant effect was observed for derivative **54**. This work also demonstrates the potential of the G5K enzyme as a biological target for the development of new anti-TB drugs.

1. Introduction

According to the World Health Organization (WHO), and despite widespread efforts to promote vaccination, early diagnosis and treatments, tuberculosis (TB) continues to be among the top 10 leading causes of death worldwide, and its causative agent, *Mycobacterium tuberculosis*, ranks second (after SARS-CoV-2) as the microorganism causing most deaths in the world [1–4]. As such, it remains a global health priority. It has been estimated that about 25% of the world's population is infected with *M. tuberculosis*, and about 10% of people may develop this illness at some point in their lives [5]. The incidence of TB among immunocompromised individuals, such as those infected with HIV, suffering from diabetes or undernutrition, is of great concern, especially its multidrug-resistant form (MDR-TB) [6,7]. Thus, the WHO reported that

* Corresponding author.
E-mail address: concepcion.gonzalez.bello@usc.es (C. González-Bello).
[1] These authors contributed equally to this work.

https://doi.org/10.1016/j.ejmech.2022.114206

about 1.4 million people died from TB in 2019, which includes 208,000 people with HIV, and about 78% of new cases were resistant to isoniazid and rifampicin, the most effective first-line TB-drugs [8,9]. Although TB is curable with a combination of 4–5 drugs, the increasing worldwide incidence of extremely resistant strains (XDR-TB), for which no treatment options are available in some cases, is a major concern in many clinical settings [10,11]. Research breakthroughs are therefore urgently needed to reduce TB incidence worldwide [12].

Throughout the history of medicine, natural products have played a crucial role in the discovery and development of new drugs, in particular anticancer and antibacterial agents [13–16]. Nature has been an amazing source of bioactive compounds, as well as highly diverse chemical entities and novel scaffolds that have allowed many natural products or naturally inspired semi-synthetic/synthetic compounds to enter into clinical use [17–19]. An analysis of drugs approved by the FDA (Food and Drug Administration) between 1981 and 2019 showed that almost 80% of new antibacterial drugs were inspired by natural products [20]. Rifampicin, which is one of the first-line TB drugs, is a good example of this. [21] In recent years, the interest in natural products as a "chemical space" source in drug discovery is re-emerging [22,23]. In this context, we became interested in exploring the therapeutic potential of Marinoquinolines for the identification of novel chemical entities with anti-TB activity. These compounds, which were isolated from diverse bacterial sources and have been largely ignored since, are 3*H*-pyrrolo[2,3-*c*]quinoline derivatives mainly substituted at the 4-position with: (i) an alkyl group, such as Marinoquinolines A (R = Me, **1**), B (R = *i*Bu, **2**), C (R = Bn, **3**), and D (R = CH_2-4-(OH)phenyl, **4**); (ii) an 1*H*-indol-3-yl group, Marinoquinoline E (**5**); or (iii) an 1*H*-indol-3-ylcarbonyl, Marinoquinoline F (**6**) (Fig. 1A) [24–26]. These compounds were found to exhibit promising antiprotozoal activity against the chloroquine-resistant strain of *Plasmodium falciparum* (K1, IC_{50}: 1.7–15 μM), and also revealed to be acetylcholinesterase inhibitors (IC_{50} values range = 3.6–8.1 μM) for the treatment of Alzheimer's disease [27]. In addition, the structurally related pyrroloquinoline alkaloid aplidiopsamine A (**7**) also proved to have promising anti-plasmodial activity against chloroquine-resistant (Dd2, IC_{50} = 1.65 μM) and chloroquine-sensitive strains (3D7, IC_{50} = 1.47 μM) of *P. falciparum* [28]. Remarkably, modifications at the 4- and 7-positions in the marinoquinoline core (compounds **8**–**40**) allowed the anti-plasmodial activity to be improved up to the nanomolar range (Fig. 1B) [29]. Thus, the most relevant example, compound **40** [^{1}R = OMe; ^{2}R = 4-(NHBoc)phenyl], was found to have an IC_{50} value of 39 nM against chloroquine-sensitive *P. falciparum* strains (3D7) and good *in vivo* activity.

Although the antibacterial activity of Marinoquinolines A–F (**1**–**6**) against pathogenic bacteria such as *Escherichia coli* and *Staphylococcus aureus* was shown to be weak (MIC >190 μM) [24], the success achieved with compound **40** resulting from modification of the 3*H*-pyrrolo[2,3-*c*]quinoline scaffold encouraged us to explore the anti-TB therapeutic potential of marinoquinoline-inspired compounds. Our interest in this scaffold was supported by the good anti-TB activity of compounds bearing a pyrrol [30] or quinoline derivative such as bedaquiline—the second-line TB-drug for the treatment of MDR-TB [1,31] and compound **41** (Fig. 1C). The latter quinoline derivative, which exhibits a MIC value of 5.5 μM against *M. tuberculosis* H37Rv and good pharmacological properties, was identified by Pitta et al. [32] by high throughput phenotypic screening of a small molecule library followed by optimization. Recently, Makafe et al. [33] identified two pyrroloquinoline derivatives, namely Z0933 and Z0930, that exhibited MIC values against *M. tuberculosis* H37Rv of 6.1 μM and 13.7 μM, respectively (Fig. 1D), by way of a whole-cell screening of an in-house chemical library of pyrroloquinoline compounds. By screening spontaneous resistant *M. tuberculosis* mutants in the presence of these compounds, the authors identified glutamate-5-kinase (G5K, 2.7.2.11), an essential enzyme in *M. tuberculosis* bacteria and involved in the proline biosynthesis pathway, as its biological target. Herein we report the synthesis of a small marinoquinoline-inspired molecule library (compounds **42**–**64**), in which positions 1, 3, 4 and 7 of the 3*H*-pyrrolo[2,3-*c*]quinoline core have been investigated, and their *in vitro* activity against *M. tuberculosis* H37Rv (Fig. 2). The structural similarity between the hit compounds identified in this study and compounds Z0933 and Z0930 led us to explore whether G5K may also be the biological target. It was found that these compounds are allosteric inhibitors of G5K. The binding modes of the most relevant compounds identified (analogs **50** and **54**), which were found to have MIC values of 4.1 and 4.2 μM, respectively, were studied by docking and then further validated by molecular dynamics (MD) simulation studies.

2. Results and discussion

2.1. Initial screening

Initially, the *in vitro* antibacterial activity of the natural marinoquinolines A (**1**), B (**2**), C (**3**) and E (**5**), as well as the previously reported synthetic marinoquinoline analogs **8**–**40** [29], was assayed by determining the minimum inhibitory concentration (MIC) against *M. tuberculosis* H37Rv using the Alamar Blue assay (Table S1) [34]. This chemical library comprised two series of compounds (series I and II), with either no substituent (^{1}R = H) or a methoxy group (^{1}R = OMe) at position 4 in the 3*H*-pyrrolo[2,3-*c*] quinoline core, respectively (Fig. 3A). Compound series I contained those ligands substituted with an aliphatic group (methyl, isobutyl, benzyl, and ethyl), whereas series II included those compounds substituted with an indole group or a phenyl moiety substituted with electron-donating (OMe, NH_2, NMe_2, Me) or electron-withdrawing groups (Cl, Br, CF_3, CO_2H, CO_2Me, NHCOMe, NHBoc). The most relevant compounds in this screening were the natural marinoquinoline B (**2**) and compound **19**, which have isobutyl (MIC = 22.6 μM) and 4-chlorophenyl (MIC = 17.9 μM) groups at position 4 in the 3*H*-pyrrolo[2,3-*c*]quinoline core, respectively (Fig. 3A). The *in vitro* antibacterial activity of compound **10**, which has benzyl and methoxy groups at positions 4 and 7, respectively, was also found to be remarkable (MIC = 34.7 μM). On the other hand, the *in vitro* activity results also revealed that the substitution of a methoxy group (electron-donating group) at position 7 in **19** decreases the antibacterial activity (MIC = 64.8 μM, Table S1), and that among the aryl groups explored in position 4, the *p*-chlorophenyl group was found to give rise to more favorable results.

These initial promising results led us to explore the possible improvement of the antibacterial activity obtained with compounds **2**, **10** and **19** by analyzing the effect of: (i) replacing the isobutyl group in **2** with an ethylenephenyl group, other branched groups (methyl-c-propyl) or a longer aliphatic chain (n-octyl); (ii) introducing electron-withdrawing groups (F, CF_3, Cl, CO_2Me) or less bulky groups (Me) in position 7 in **19** and in derivatives such as **2**; and (iii) functionalizing the 1-position in the 3*H*-pyrrolo [2,3-*c*] quinoline core (Cl, Br, aryl group) (Fig. 3B). In addition, the need for a free NH group in the marinoquinoline-inspired scaffold was also explored. To this end, compounds **42**–**64** were synthesized, as discussed below.

2.2. Synthesis of compounds 42–64

Compounds **42**–**50** and **52**–**56**, which contain a free NH group, were prepared as outlined in Scheme 1. Synthesis was achieved in

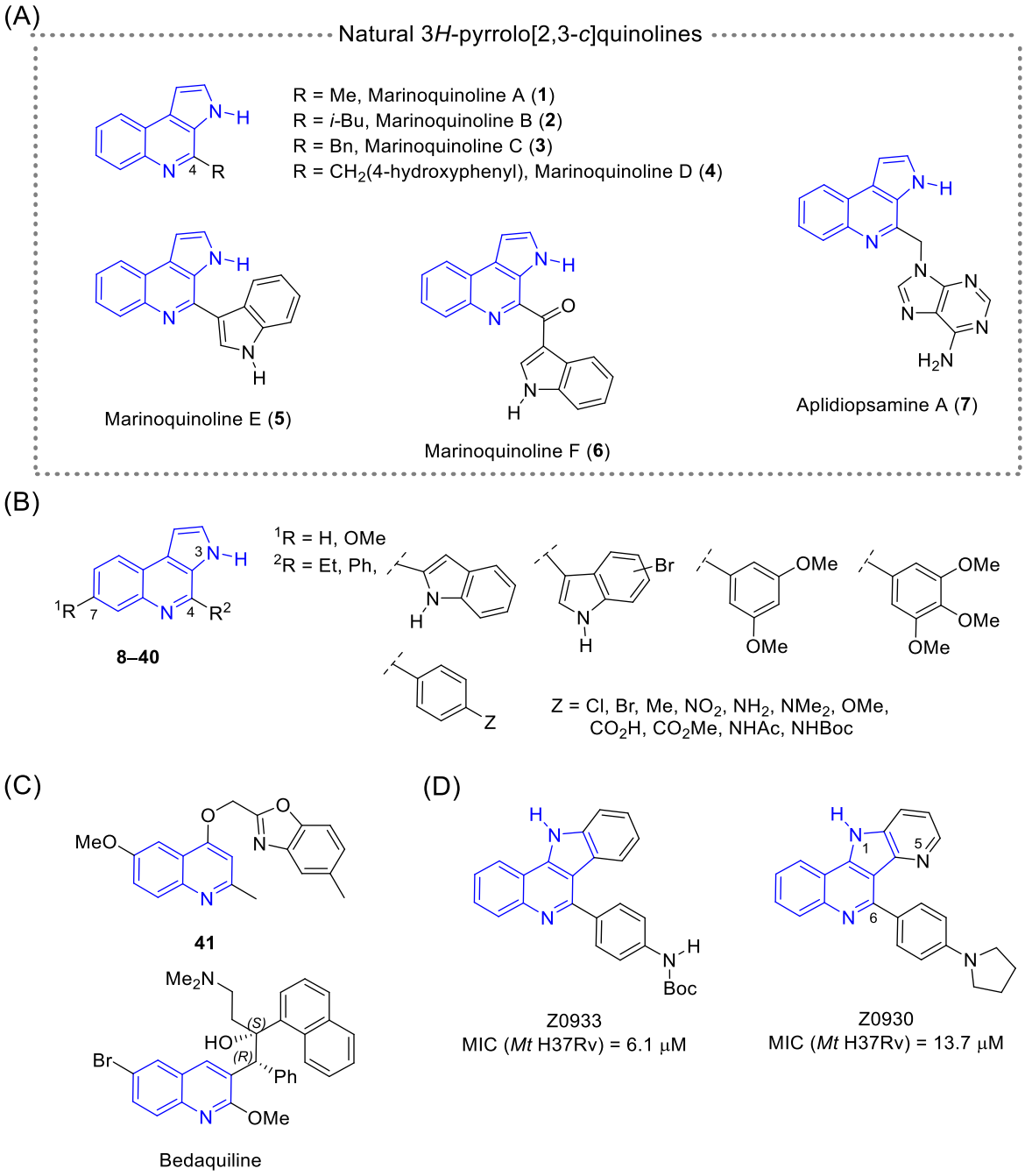

Fig. 1. (A) Natural 3*H*-pyrrolo[2,3-*c*]quinolines. (B) Marinoquinoline-inspired derivatives **8**–**40** obtained by synthesis that led to the identification of a potent and fast-acting *P. falciparum* inhibitor with *in vivo* activity. (C) Selected quinoline-based compounds active against *M. tuberculosis* H37Rv. (D) Identified 11*H*-indolo[2,3-*c*]quinoline derivatives Z0933 and Z0930 that kill *M. tuberculosis* H37Rv by activation of glutamate-5-kinase enzyme.

three steps from commercially available 3-(4,4,5,5-tetramethyl [1–3]dioxaborolan-2-yl)-1-(triisopropylsilanyl)-1*H*-pyrrole (**65**), as reported previously on a large scale [29,35–37]. The first step consisted of the Suzuki–Miyaura cross-coupling reaction between pyrrole boronate ester **65** and the corresponding bromoaniline derivatives using catalytic amounts of $Pd(OAc)_2$ and SPhos and in the presence of K_2CO_3. This led to pyrroloanilines **66**–**71**, with isolated yields ranging from 68% to 93%. Secondly, deprotection of the TIPS groups in **66**–**71** with TBAF efficiently afforded pyrroloanilines **72**–**77**. Finally, the Pictet–Spengler cyclization of pyrroloanilines **72**–**77** and previously reported compound **78** [29] using the corresponding aliphatic and aromatic aldehydes (1.2 equiv.) and trifluoroacetic acid (1 equiv.) gave the desired marinoquinoline-inspired analogs **42**–**50** and **52**–**56** with isolated yields ranging from 23% to 78%.

The amino moiety of compounds **19**, **54**, **57** and **50** was then functionalized with a methyl or a methylcyclopropyl group (Scheme 2). The new analogs (compounds **58**–**61** and **51**) were synthesized by treatment of compounds **19**, **54**, **57** and **50** with sodium hydride, followed by reaction with iodomethane or (iodomethyl)cyclopropane (yields ranged from 39% to 75%). Furthermore, regioselective chlorination of position 1 in **19** was achieved

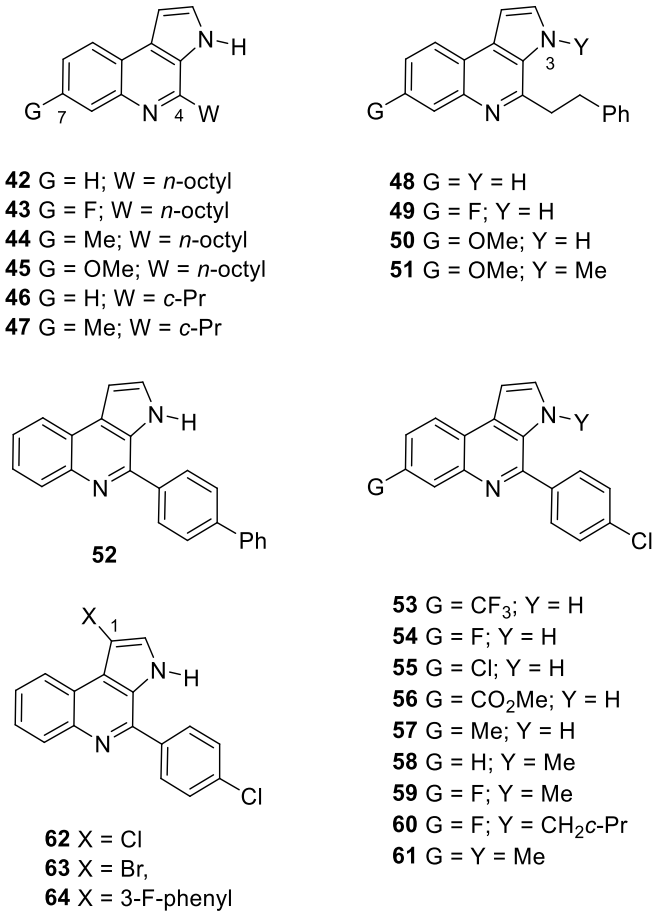

Fig. 2. Synthetic 3*H*-pyrrolo[2,3-*c*]quinoline derivatives **42**–**64** explored for the identification of new anti-TB compounds.

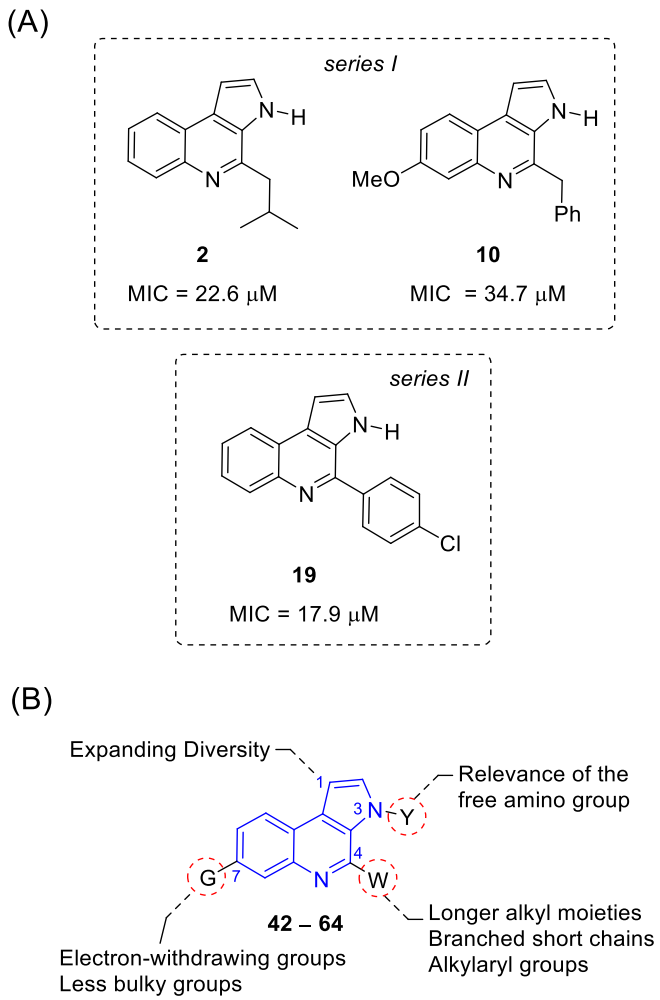

Fig. 3. A. Most active natural and previously reported synthetic 3*H*-pyrrolo[2,3-*c*] quinoline derivatives against *M. tuberculosis* H37Rv identified in the first screening. B. Positions of the 3*H*-pyrrolo[2,3-*c*]quinoline scaffold explored for optimization (compounds **42**–**64**).

by treatment with *N*-chlorosuccinimide at high temperature to give compound **62** in 64% isolated yield. Similarly, bromide **63** was prepared from **19** in 79% isolated yield using *N*-bromosuccinimide at room temperature. Finally, a Suzuki cross-coupling reaction between bromide **63** and (3-fluorophenyl)boronic acid in the presence of K_2CO_3 and $Pd(PPh_3)_4$ as catalyst gave compound **64** in 42% isolated yield.

2.3. *In vitro* anti-tuberculosis activity of compounds 42–64

The *in vitro* antibacterial activity of compounds **42**–**64** against *M. tuberculosis* H37Rv was then measured; the MIC values obtained are summarized in Table 1. The results with compounds **2** and **10** (series I) and **19** (series II) from the aforementioned initial screening are also included in Table 1 for comparison.

The results obtained with derivatives from series I (compounds **42**–**51**), which possess an aliphatic chain in the 4-position of the pyrroloquinoline scaffold (Table 1, entries 3–12), revealed that, in general, substitution of the position 7 by a methoxy group enhanced the antibacterial activity. In addition, the replacement of the isobutyl group in marinoquinoline B (**2**, MIC = 22.6 μM; Table 1, entry 1) by an n-octyl group (compounds **42**–**45**) improved the antibacterial activity slightly, irrespective of whether the substituent at the 7-position was an electron-withdrawing or electron-donating group (MICs values ranged between 16.1 and 17.8 μM) (Table 1, entries 3–6), and no significant enhancement was observed in those compounds bearing a *c*Pr group (compounds **46**–**47**; Table 1, entries 1 vs entries 7 and 8). In contrast, a remarkable positive effect was obtained upon replacement of the benzyl group in **10** by an ethylenephenyl group (compound **50**), which led to a nine-fold improvement in the *in vitro* activity (MIC = 4.1 μM; Table 1, entries 2 *vs* 11). Finally, the presence of the methoxy group in the ethylenephenyl pyrroloquinoline **50** proved to be relevant for increasing *in vitro* activity, since a lack of the latter group or its substitution by a fluoride [compounds **48** (MIC = 36.7 μM) and **49** (MIC = 34.4 μM)] resulted in a marked loss of activity (Table 1, entries 9 and 10 *vs* 11).

On the other hand, the results obtained with the new derivatives in series II functionalized with an aryl group at the 4-position of the pyrroloquinoline scaffold (compounds **52**–**64**; Table 1, entries 14–26) suggested a distinct trend from compounds derived from series I. The introduction of a fluoride or a methyl group at position 7 in the tricyclic system, instead of a methoxy group, proved to be key to improving the *in vitro* activity. Thus, compounds **54** and **57** provided the best results, showing MIC values of 4.2 and 8.5 μM, respectively (Table 1, entries 16 and 19).

Moreover, in general, alkylation of the NH group caused a reduction in the *in vitro* activity of between two- and three-fold. Thus, the introduction of a *c*Pr group at the NH group in **54** (compound **60**) and a methyl group in ethylenephenyl pyrroloquinoline

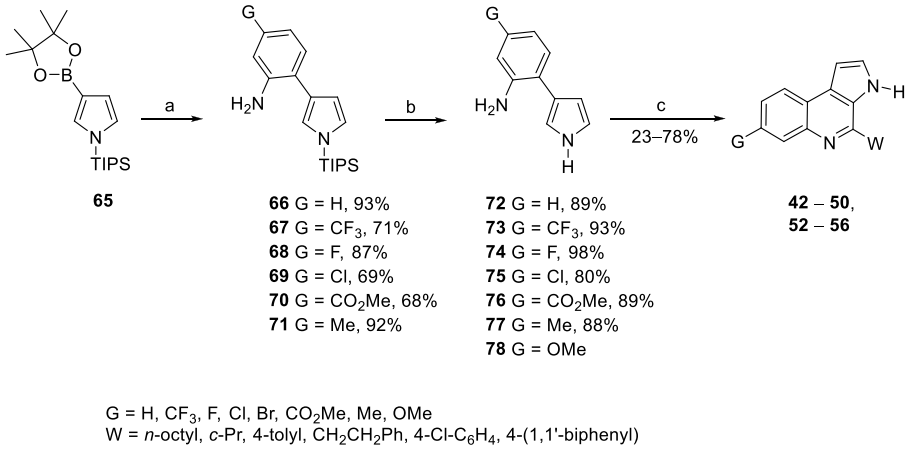

Scheme 1. Synthesis of compounds **42**–**50**, **52**–**56**. *Reagents and conditions*: (a) corresponding bromoaniline, $Pd(OAc)_2$ (cat), SPhos, K_3PO_4, *n*BuOH/H_2O, 80 °C. (b) TBAF, THF, RT. (c) RCHO, TFA, CH_2Cl_2, RT.

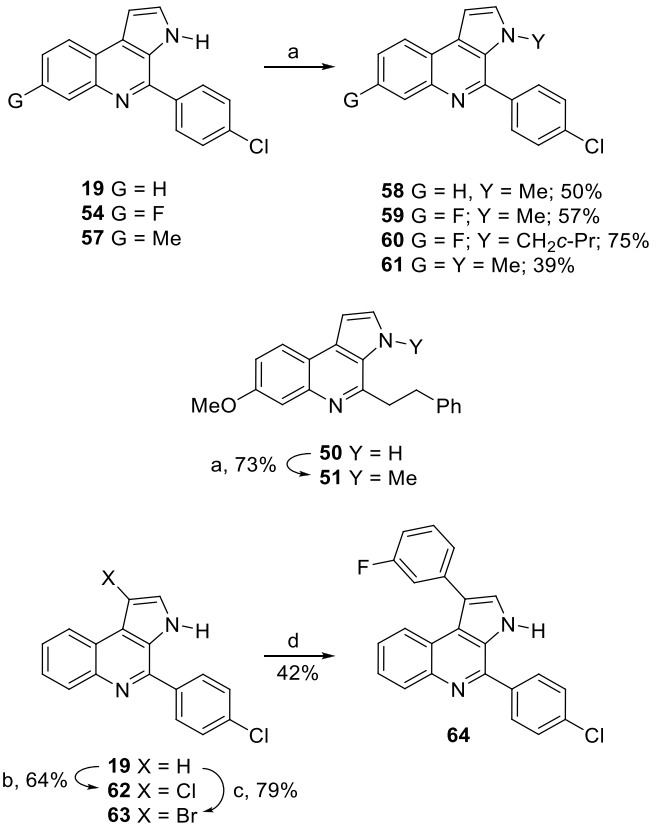

Scheme 2. Synthesis of compounds **58**–**64**. *Reagents and conditions*: (a) 1. NaH, THF, 0 °C. 2. MeI or (iodomethyl)cyclopropane, RT. (b) NCS, DMF, Δ. (c) NBS, THF/H_2O, RT. (d) (3-fluorophenyl)boronic acid, $Pd(PPh_3)_4$, K_2CO_3, dioxane/H_2O, 90 °C.

50 (compound **51**) resulted in an increase in the MIC values from 4.2 to 14.2 μM and from 4.1 to 7.9 μM, respectively (Table 1, entries 22 and 12 *vs* 16 and 11). Despite this increase, the values achieved are lower than those obtained for many of the compounds with a free NH group, such as Marinoquinoline B (**2**, MIC = 22.6 μM).

Furthermore, while the introduction of a halide (Cl, Br) at position 1 in **19** (MIC = 17.9 μM) had a positive impact on the *in vitro* activity (compound **62**, MIC = 16.0 μM; compound **63**, MIC = 14.0 μM, Table 1, entries 13 *vs* 24 and 25), the incorporation of an aromatic group at the same position resulted in a decrease in the *in vitro* activity (compound **64**, MIC = 26.8 μM, Table 1, entries 26 *vs* 25). In summary, we have identified two compounds based on the natural marinoquinoline scaffold, namely analogs **50** and **54**, with good *in vitro* activity against *M. tuberculosis* H37Rv (MIC values of 4.1 and 4.2 μM, respectively).

2.4. Enzymatic assays

Makafe et al. [33] identified two pyrroloquinoline derivatives, namely Z0933 and Z0930 (Fig. 1), that exhibit *in vitro* activity against *M. tuberculosis* H37Rv with MIC values of 6.1 and 13.7 μM, respectively, by inhibition of G5K enzyme. G5K is an essential enzyme for *M. tuberculosis*, encoded by the *Rv2439c* gene (also named *proB*), that is involved in the first step of the proline biosynthesis pathway [38–42]. G5K catalyzes the phosphoryl-transference of the γ-phosphate group of ATP to L-glutamate (L-Glu) to provide L-glutamyl-5-phosphate and ADP, and also regulates the synthesis of L-proline (L-Pro), which is involved in protecting the cell against osmotic stress, by feed-back inhibition by L-Pro [43,44] Z0933 and Z0930 appeared to cause an allosteric activation of G5K, which results in an increase in L-Pro levels, thus causing a redox imbalance and an accelerated production of reactive oxygen species that finally kill the bacterium. The pyrroloquinoline core and the phenyl substituent at the 6-position of Z0933 and Z0930 were found to be essential for enhancing the activity of G5K. The authors suggested that these compounds may interact with *M. tuberculosis* G5K (*Mt*-G5K) in the vicinity of residue Ala266, which is located on the amino acid kinase (AAK) domain (residues 1–264). However, details of the binding mode of compounds Z0933 and Z0930 at an atomic level, as well as how this allosteric activation is achieved, were not provided.

The structural similarity between the hit compounds identified in this study and compounds Z0933 and Z0930 led us to explore whether *Mt*-G5K may also be the biological target for the compounds **50** and **54**. To this end, the enzymatic activity of *Escherichia coli* G5K (*Ec*-G5K) was evaluated in the presence of compounds **50** and **54**, which proved to have lower *in vitro* activity against this pathogen (eight-fold). Enzyme assays at fixed substrate and enzyme concentrations in the absence and presence of various concentrations of compounds **50**, **54** and L-Pro, which is its natural inhibitor, were performed. Analogs **50** and **54** were found to inhibit *Ec*-G5K. At 10 mM concentration of both substrates (ATP, L-Glu), the estimated $I_{0.5}$ values were 22.1 ± 0.7 and 33 ± 12 μM, respectively,

Table 1
Minimum inhibitory concentration (MIC) of compounds **42**–**64** against *M. tuberculosis* H37Rv[a].

Series	Entry	Compd.	W	G	X	Y	MIC (μM)
I	1	**2**	*i*-Bu	H	H	H	22.6
I	2	**10**	Bn	OMe	H	H	34.7
I	3	**42**		H	H	H	17.8
I	4	**43**		F	H	H	16.8
I	5	**44**		Me	H	H	17.0
I	6	**45**		MeO	H	H	16.1
I	7	**46**		H	H	H	24.0
I	8	**47**		Me	H	H	45.0
I	9	**48**		H	H	H	36.7
I	10	**49**		F	H	H	34.4
I	11	**50**		MeO	H	H	4.1
I	12	**51**		MeO	H	Me	7.9
II	13	**19**	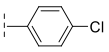	H	H	H	17.9
II	14	**52**	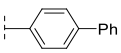	H	H	H	31.2
II	15	**53**	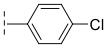	CF_3	H	H	14.4
II	16	**54**	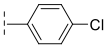	F	H	H	4.2
II	17	**55**	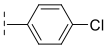	Cl	H	H	16.0
II	18	**56**	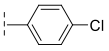	CO_2Me	H	H	>500
II	19	**57**	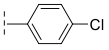	Me	H	H	8.5
II	20	**58**	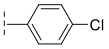	H	H	Me	17.1
II	21	**59**	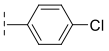	F	H	Me	ND
II	22	**60**	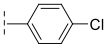	F	H		14.2
II	23	**61**	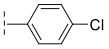	Me	H	Me	16.3
II	24	**62**	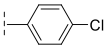	H	Cl	H	16.0
II	25	**63**	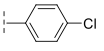	H	Br	H	14.0
II	26	**64**	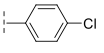	H		H	26.8

[a] MIC value for the reference drug moxifloxacin = 0.15 μM.

where $I_{0.5}$ is the concentration causing 50% inhibition (Fig. 4A). Under the same assay conditions, the calculated $I_{0.5}$ value for L-Pro was 2.5 ± 0.3 μM. Unlike L-Pro and compound **50**, derivative **54** proved to inhibit only partially the enzyme, thus suggesting that this compound produces a partially active complex. By extrapolation of the remaining activity at ∞ concentration of compound **50**, the residual enzyme activity was estimated to be of 41%. Moreover, the two analogs **50** and **54** were found not to compete for the L-Pro binding site as the inhibitory capacity of L-Pro was not altered by the presence of compounds **50** (50 μM) and **54** (40 μM) (Fig. 4B). These results suggest that G5K may also be the target for compounds **50** and **54**. At 10 mM concentration of L-Glu and ATP, $I_{0.5}$ values for L-Pro, compounds **50** and **54** were 2.5 ± 0.3 μM, 22.1 ± 0.7 μM and 33 ± 12 μM, respectively.

The effects on the K_m^{app} and V_{max}^{app} for ATP at constant concentrations of L-Glu (150 mM, 300 mM and 600 mM) and ATP (10 mM) in the presence and absence of compounds **50** (120 μM) and **54** (120 μM) were then studied. For these assays, higher concentrations of L-Glu were employed because at the previously concentration used (10 mM) the kinetic data for ATP was adjusted to a sigmoid with a very high slope, which made it difficult to quantify the effect of the inhibitors on kinetic parameters (Fig. S1A). Fortunately, under these assay conditions, the kinetic data for ATP was fitted to a hyperbole with more suitable values for quantifying the plausible changes in K_m^{app} and V_{max}^{app} values. As before, L-Pro and compound **50** caused the total inhibition of the *Ec*-G5K enzyme, while partial inhibition (~40%) was obtained with compound **54** (Fig. S1B). For all cases, higher $I_{0.5}$ values were observed. The results revealed that compound **50** caused a substantial increase in the K_m^{app} for ATP, while no significant effect was identified for derivative **54** (Fig. 5A). For compound **50**, no relevant effects on the V_{max}^{app} for ATP were identified, while these velocities were somewhat lower in the presence of derivative **54** (Fig. 5B). The effect on the K_m^{app} for ATP caused by compound **50** explains the inhibition obtained in the assays using 150 mM of L-Glu and 10 mM of ATP (Fig. S1B), since the activity observed in the presence of **50** (68% of the activity without inhibitor) is very similar to that expected for the observed increase in K_m^{app} for ATP from 2.2 to 8.4 mM (66% of the expected relative activity). It is worth highlighting that while the active site of G5K enzyme is highly conserved, there are significant differences in the amino acid sequence between homologous enzymes (Fig. S2). Therefore, differences in the binding affinity of the reported compounds against *Mt*-G5K and *Ec*-G5K are expected. Taken together, these outcomes suggest that the inhibition of the G5K enzyme by compound **50** is due to the reduction of the binding affinity of ATP for catalysis. In contrast, compound **54** would inhibit this enzyme by preventing the binding of L-Glu, which would be discussed below.

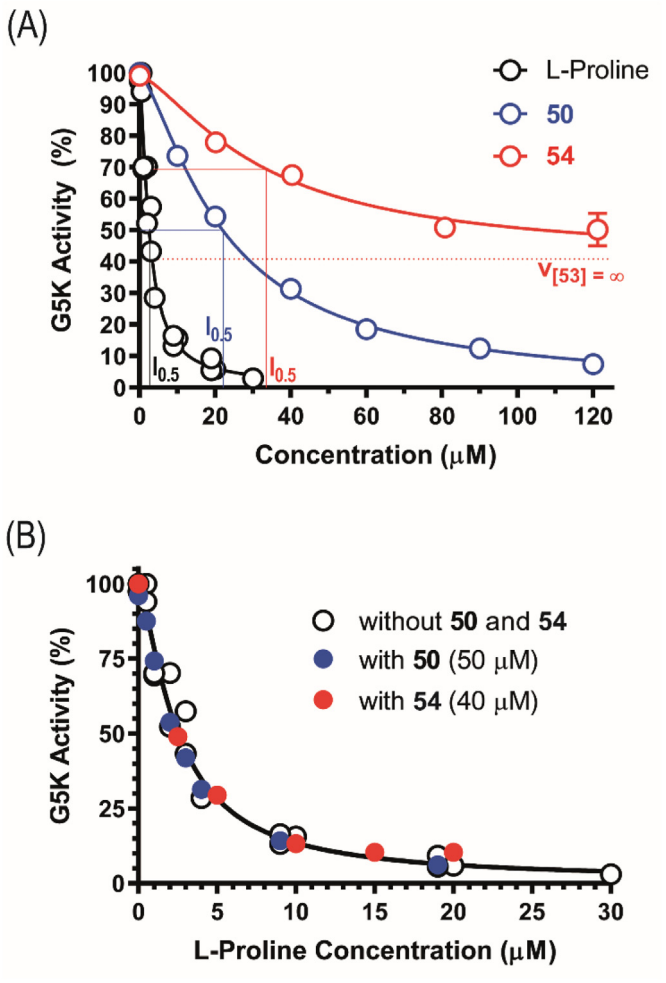

Fig. 4. (A) Activity of *Ec*-G5K in the presence of increasing concentration of compounds **50**, **54** and L-Pro. (B) Effect on the inhibition of *Ec*-G5K by L-Pro in the presence of compounds **50** (50 μM) and **54** (40 μM). Assay results are given as the means ± S.E. of at least three determinations.

2.5. Cytotoxicity assays

The cytotoxicity of inhibitors **50** and **54** in the HepG2 cell line (human hepatocellular carcinoma) was evaluated using the MTT [3-(4,5-dimethylthiazol-2-yl)-2,5-diphenyltetrazolium bromide] assay by calculating the percentage of inhibition of cell growth induced by various concentrations (5 μM, 10 μM and 20 μM) of compounds **50** and **54**. The results showed that no relevant cytotoxicity was exhibited by both compounds (Table 2).

2.6. Molecular dynamics simulation studies

2.6.1. Compounds binding mode

To gain an insight into how the hit compounds identified in this study may inhibit G5K enzyme at the molecular level, computational studies were carried out with the two homologous enzymes, *Ec*-G5K and *Mt*-G5K. For *Ec*-G5K, the available crystal structures PDB ID 2J5T, which has L-Glu and sulfate in the active site, and PDB ID 2J5V, which is in complex with L-glutamyl-5-phosphate and pyroglutamic acid, were employed [45]. Unsolved residues were modelled using the web-based ModLoop server [46]. For the *M. tuberculosis* enzyme, as no three-dimensional structure of *Mt*-G5K is available, a homology model was constructed using the homology modelling web-based Phyre2 server and further validated by MD simulation studies [47]. The constructed three-dimensional structure of *Mt*-G5K showed to be very stable as *Ec*-G5K. Thus, the analysis of the root-mean-square deviation (rmsd) for the whole protein backbone (C_α, C, N and O atoms) calculated in the unbound form of *Mt*-G5K and *Ec*-G5K enzymes obtained from MD simulations studies revealed that it varies relatively low (Fig. S3). For the AAK domain, average values of 3.45 Å (*Mt*-G5K) and 2.06 Å (*Ec*-G5K) were obtained, while for the PUA domain, values of 2.70 Å (*Mt*-G5K) and 0.83 Å (*Ec*-G5K) were identified. Remarkably, for *Mt*-G5K, the protein region close to the ATP binding site is more flexible than for *Ec*-G5K.

With both three-dimensional structures in hands, the binding mode of compounds **50** and **54** was explored by molecular docking using GOLD [48] version 2020.2.0 and further studied by MD simulation studies. These types of computational studies, in which

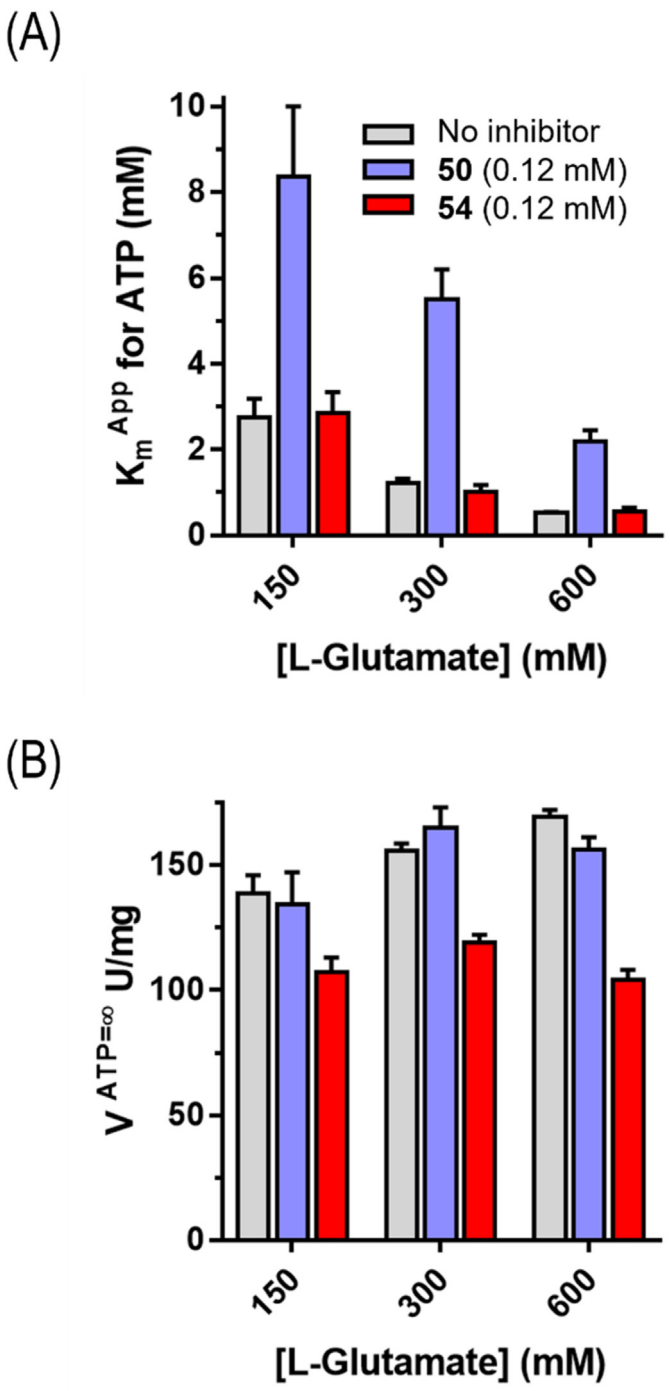

Fig. 5. Variation of the K_m^{app} (A) and V_{max}^{app} (B) for ATP in the reaction catalyzed by *Ec*-G5K at three L-Glu concentrations (150 mM, 300 mM, and 600 mM) in the presence and absence of compounds **50** (0.12 mM) and **54** (0.12 mM). Assay results are given as the means ± S.E. of at least three determinations.

both the ligand and the macromolecule are considered flexible, are complementary tools widely used in drug discovery and drug-design programs to explore and/or validate potential binding modes and are usually obtained via molecular docking studies in which the macromolecule is considered as a rigid template (lock-key model) [49,50]. As a result, the outcomes of these docking studies will be driven by the target conformation employed, which is commonly obtained from available three-dimensional structure(s) or homology models constructed from the latter. However,

Table 2
Cytotoxicity data of compounds **50** and **54** on HepG2 cells.[a].

Compound	Concentration (μM)	% cell growth inhibition
50	5	1 ± 1
	10	3 ± 2
	20	17 ± 3
54	5	1 ± 2
	10	1 ± 2
	20	2 ± 2

[a] Cisplatin (control): IC_{50} = 6.3 ± 0.1 μM, % inhibition = 63 ± 2.

the enzyme conformation is generally induced by the ligand/substrate that it recognizes, thereby maximizing the ligand—enzyme interactions (induced-fit model), and may be markedly different from that adopted with the compounds used for crystallization, or in the unbound form. Indeed, the biological function of an enzyme depends on both its three-dimensional structure and its intrinsic-shape motion for turnover, that is, on its "conformational state". As a result, the ligand-binding mode proposed by docking studies using unrealistic enzyme conformations may be an artifact, or quite different from the real ligand@enzyme complex, since the plasticity of the macromolecule has not been considered. This fact is particularly relevant for allosteric interactions that usually promote new arrangements across the protein backbone to achieve long-distance conformational changes that modify the intrinsic catalytic activity. Hence, a study of the ligand@enzyme complexes obtained by docking using dynamic simulations allows false binding modes, in which case the ligand would escape from the pocket (unstable), to be ruled out, and a more realistic picture of the effects caused by the ligand on an atomic scale to be obtained.

G5K enzyme has two domains: AAK (amino acid kinase, residues 1—264 in *Mt*-G5K), which contains the catalytically active site (catalysis and pathway modulation), and PUA (pseudouridine synthase and archaeosine transglycosylase, residues 281—376 in *Mt*-G5K), the function of which is still unclear. Although the PUA domain is not required for substrate binding, catalysis, or regulation, it seems to play some role in modulating the properties of the enzyme [45]. Based on the structural similarity between compounds **50** and **54** and Z0933 and Z0930, we hypothesized that the compounds reported herein may interact in the same enzyme region, i.e. the interdomain interface, which was selected for docking. The **50**@G5K and **54**@G5K enzyme complexes obtained by docking were inmersed in a truncated octahedron box of water molecules and then subjected to 100 ns (200 ns in some cases) of dynamic simulation for validation using the molecular mechanics force field AMBER ff14SB and GAFF. The results of these studies showed that both compounds interact with the interface between enzyme domains, but in different pockets, as expected for aromatic compounds with markedly different electron densities and overall architectures. Thus, while analog **50** is an electron-rich pyrroloquinoline containing apolar and conformationally flexible substituents, compound **54** is an electron-deficient system containing electronegative substituents and a phenyl group.

Compound **54** binds in the allosteric site close to the L-Glu binding site. For the *Mt*-G5K enzyme, this pocket is formed by helix αE, αG and αH of the AAK domain and helix αJ of the linker that joins the two enzyme domains (Fig. 6A). Compound **54** establishes two main polar interactions with the enzyme: (i) a hydrogen-bonding interaction between the guanidinium group of residue R159 and the quinoline nitrogen atom of the ligand and (ii) a cation-π interaction between the guanidinium group of R159 and the 4-chlorophenyl moiety. In addition, diverse lipophilic contacts, such as halogen-CH interactions with residues A113, F154 and A226, and CH-π interactions with residues L163 and L230, were

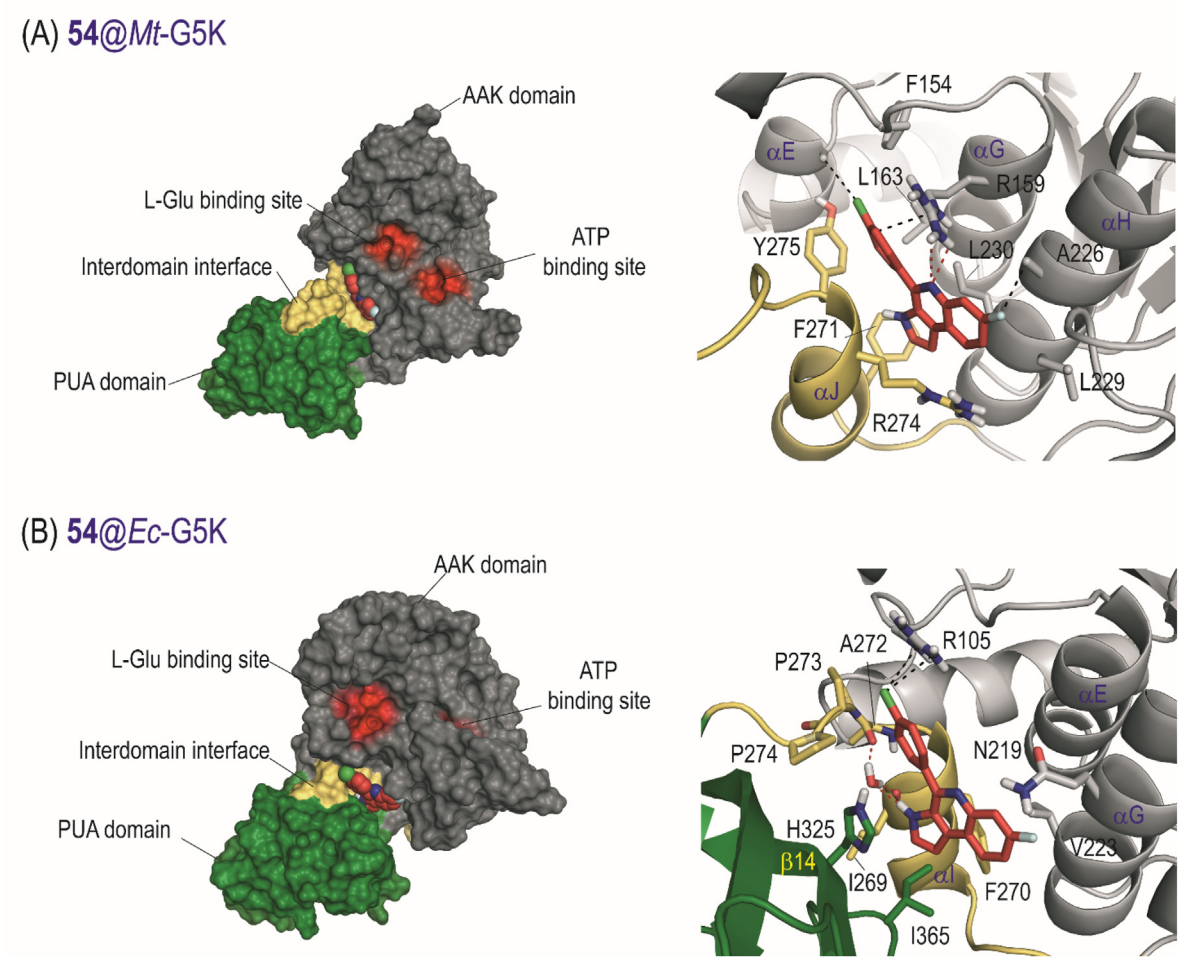

Fig. 6. Binding mode of compound **54** against *Mt*-G5K (A) and *Ec*-G5K (B) obtained by MD simulation studies. Overall and detailed views are provided. Snapshots taken after 90 ns and 100 ns of simulation, respectively. The AAK and PUA domains and the interdomain interfaces are shown in gray, green, and yellow, respectively. In the surface representation, the positions of the L-Glu and ATP binding sites are highlighted in red. Relevant side-chain residues are shown and labeled. Hydrogen bonding (red) and cation-π stacking and/or halogen-CH (black) interactions are shown as dashed lines.

identified. For *Ec*-G5K enzyme, a similar arrangement of compound **54** was observed (Fig. 6B). In this case, the inhibitor interacts with the linker through the residues I269, F270, P273 and P274, with the AAK domain via the residues V223 and N219, and with the PUA domain with the residues H325 and I365. For both G5K enzymes, compound **54** proved to be stable within the pocket as no relevant changes were observed during the whole simulation, either in the location of the ligand (Fig. S4) nor the overall enzyme complex (Fig. S5).

Although compound **50** also interacts with the interface between domains, the targeting allosteric site is located close to the ATP binding site (Fig. 7). For the *Mt*-G5K enzyme, compound **50** interacts with the pocket created by helix αH (AAK domain) and αJ (linker) and β-sheets β6, β7 and β9 (AAK domain). This is an arginine-rich region (R212, R262) that captures the electron-rich pyrroloquinoline ring of **50** by forming cation-π interactions between both faces of this ring and the guanidinium groups. Compound **50** is further anchored within the pocket via numerous lipophilic interactions with the apolar residues in the vicinity, specifically residues V209, A210, L229, L230, A226 and A232. For the *Ec*-G5K enzyme, although the targeting allosteric site is the same, the arrangement of the ligand within the pocket is slightly different, mainly caused by the differences in both the length and folding of this flexible region of both homologous enzymes. Specifically, compound **50** would bind to the pocket created by helix αF and αG, as well as the loop that connects them (AAK domain), and the loop that joins the β-sheets β14 and β16 (PUA domain). This allosteric inhibitor would be anchored to this site by two strong polar interactions, thus a strong cation-π interaction between the tricyclic system and the guanidinium group of R321 and a hydrogen bonding interaction between the NH moiety and the main-chain carbonyl group of E319. Compound **50** would be further stabilized in the pocket thanks to numerous lipophilic interactions with residues I194, L198, L218, L209, as well as the carbon side-chains of D195 and N219. In any case, as for compound **54**, the stability of compound **50** within this allosteric site close to the ATP binding site of both enzymes is remarkable as no relevant changes were observed during the whole simulation (Figs. S4 and S5).

2.6.2. Allosteric control

To determine the long-distance conformational changes induced by the interaction of compounds **50** and **54** at the interface between domains of the G5K enzyme on the enzyme active site, and the impact thereof on enzymatic activity, binding of the natural substrates (L-Glu, ATP-Mg^{2+}) in the absence (Michaelis complex) and in presence of these inhibitors was explored *in silico*. To this end, the dynamic behaviour of: (i) the Glu + ATP-Mg^{2+}@G5K

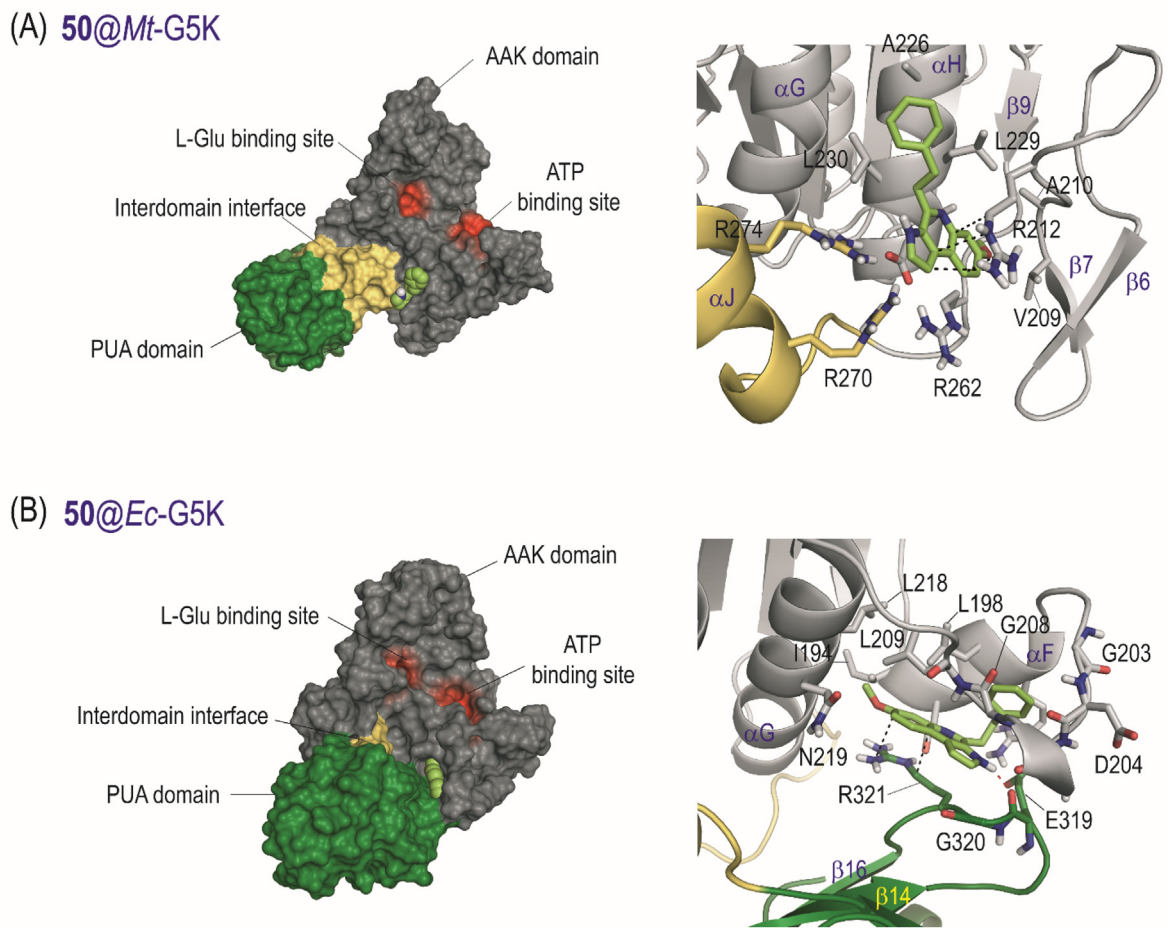

Fig. 7. Binding mode of compound **54** against *Mt*-G5K (A) and *Ec*-G5K (B) obtained by MD simulation studies. Overall and detailed views are provided. Snapshots taken after 190 ns and 100 ns of simulation, respectively. The AAK and PUA domains and the interdomain interfaces are shown in gray, green, and yellow, respectively. In the surface representation, the positions of the L-Glu and ATP binding sites are highlighted in red. Relevant side-chain residues are shown and labeled. Hydrogen bonding (red) and cation-π stacking and/or halogen-CH (black) interactions are shown as dashed lines.

tertiary enzyme complexes; and (ii) the enzyme complexes obtained after addition of the natural substrates to the aforementioned **50**@G5K and **54**@G5K binary complexes, was studied, which is discussed below.

Generating the G5K Michaelis complex model did not turn out to be an easy task, due to the lack of information in atomic detail about the bioactive conformation of ATP, which is its magnesium chelate, ATP-Mg^{2+}. Although the binding modes of L-Glu and ADP (product) are available in the crystal structures of *Ec*-G5K (PDB ID 2J5T, 2.9 Å, [45]) and the AAK domain of G5K from *Campylobacter jejuni* (PDB ID 2AKO, 2.2 Å, [51]), respectively, the identification of the disposition of the γ-phosphate of ATP and its coordination with Mg^{2+} was not obvious. All attempts made using the predominant geometries for ATP-Mg^{2+} in the PDB, in which Mg^{2+} is coordinated by both the β- and γ-phosphates or by all three phosphate groups concurrently, failed [52]. Our studies revealed that for G5K Mg^{2+} is coordinated by both the α- and γ-phosphates of ATP, which is also observed in some ATP-dependent enzymes (see for example PDB ID 5O26, [53]).

These computational studies revealed that glutamate binds at the active site of *Mt*-G5K by forming direct and indirect contacts with several conserved residues, mainly *via* the side chains, the main NH groups of these residues, and a network of water molecules (Fig. 8A). Specifically, the amino group in the substrate establishes three hydrogen-bonding interactions with three conserved residues (motif NEND): one with the carbonyl group of the side chain of N142, and two with the terminal carboxylate group of E143 and of D145 *via* two water molecules. The carboxylate group close to the amino group in L-Glu establishes four hydrogen bonds with four conserved residues: three with the main NH groups of residues A60, I61, and A62 (motif SGAIA), and another with the NH_2 group of the side-chain in residue N142. Remarkably, the binding of L-Glu freezes the arrangement of this conserved motif, probably to fix the conformation of L-Glu at the active site to enhance the phosphoryl-transfer reaction by ATP. Finally, the terminal carboxylate group interacts by hydrogen-bonding with the main NH group of the conserved residue N157, as well as with diverse residues *via* a network of water molecules. A similar arrangement of L-Glu was also observed in the *Ec*-G5K Michaelis complex, which is also coincident with the observed in PDB ID 2J5T (Fig. 8B).

For both enzymes, ATP-Mg^{2+} is anchored in the ATP binding site through numerous electrostatic and hydrogen-bonding interactions with diverse conserved residues, many of them involving the triphosphate moiety. Specifically, the triphosphate group in ATP, in addition to the chelation with Mg^{2+}, interacts with the bottom part of the active site through the residues K18/K10, K224/K217, S58/S50, and D158/D150 (in *Mt*-G5K and *Ec*-G5K,

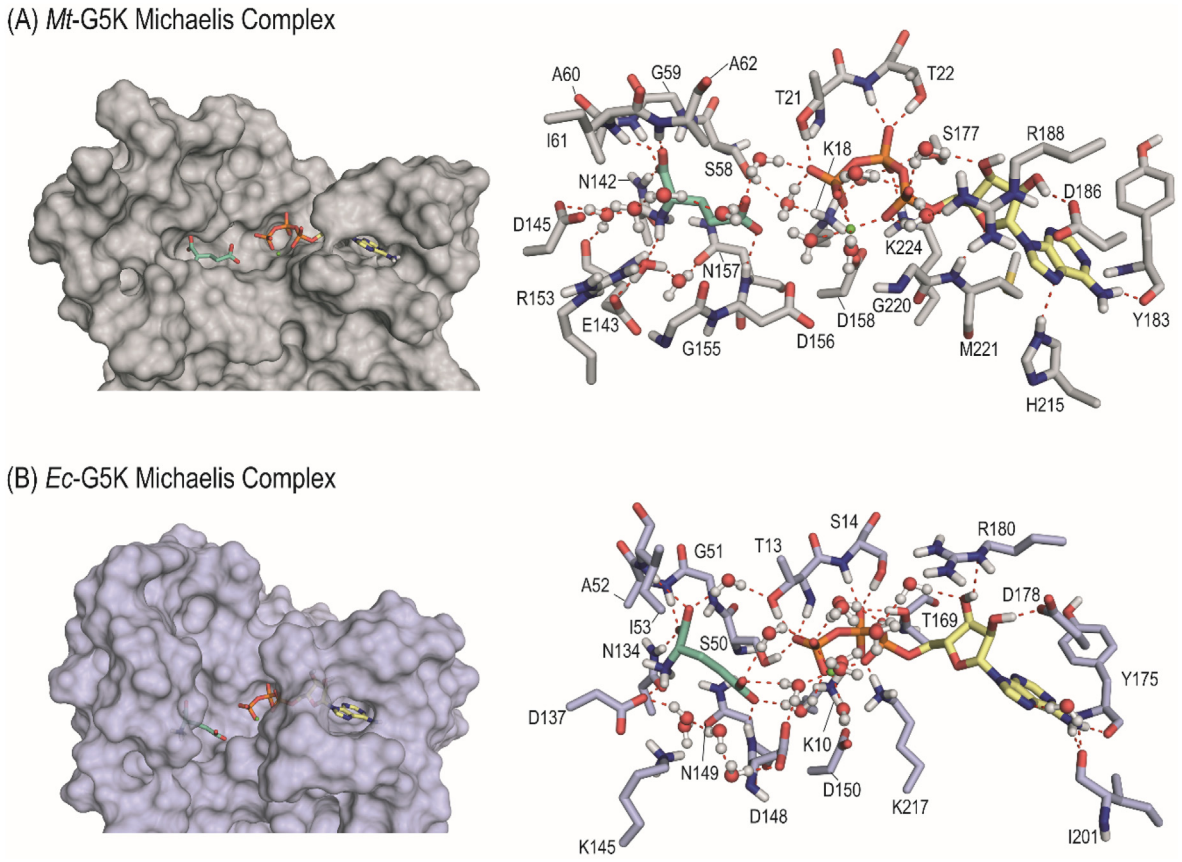

Fig. 8. Michaelis complexes from *Mt*-G5K (A) and *Ec*-G5K (B) complex obtained by MD simulation studies. Overall and detailed views are provided. Snapshots taken after 80 ns and 20 ns of simulation, respectively. The relevant residues, side chains, and water molecules involved in the substrates (L-Gu, ATP) binding are shown and labeled. Hydrogen-bonding and electrostatic interactions are indicated as red dashed lines. Mg^{2+} is shown as a green sphere.

respectively), as well as with the residues T21/T13 and T22/S14 (in *Mt*-G5K and *Ec*-G5K, respectively), which are located on one site of the active site (Fig. 8). The position of the ribose ring in ATP is fixed thanks to hydrogen-bonding interactions between its hydroxyl groups and the side chains of the conserved residues D186/D178 and R188/R180 (in *Mt*-G5K and *Ec*-G5K, respectively), as well as diverse contacts with a network of water molecules. Finally, the adenine moiety binds at the active site through hydrogen-bonding interactions between its amino group and the main carbonyl group of Y183/Y175 (in *Mt*-G5K and *Ec*-G5K, respectively) and either the side chain of H215 (*Mt*-G5K) or the main carbonyl group of I201 (*Ec*-G5K). Under this arrangement, both Michaelis complexes proved to be stable. Thus, the analysis of the root-mean-square deviation (rmsd) for the ligand(s) calculated in both complexes, as well as the variation of the relative distance between the atoms involved in the most relevant interactions, revealed that the substrates are well anchored in the active site during the whole simulation (Figs. S6 and S7).

Once the active conformation of G5K was determined, as well as the L-Glu and ATP-Mg^{2+} binding modes, the possible conformational changes of the active site induced by the binding of compounds **50** and **54**, their effects on the binding of L-Glu and ATP and therefore on the ability of the enzyme to catalyze the phosphoryl-transfer reaction, were studied. To this end, the binding of the substrates to the **50**@G5K and **54**@G5K binary complexes was explored, and the dynamic behaviour of the resulting complexes analyzed. The results showed that these compounds have different effects on the enzyme conformation and shape-motion, as expected from ligands binding to separate sites, which are close to distinct catalytic sites of the target. Thus, the binding of compound **54** promotes marked conformational changes in the L-Glu binding site, while ATP (as well as **54**) is stable in its corresponding pocket. This results in destabilization of the L-Glu in the active site, which is expelled from the active site while ATP remains stable (Fig. 9A). For the *Ec*-G5K, this process was observed almost at the beginning of the simulation. Taken together, the binding of compound **54** appears to induce relevant conformational changes at the L-Glu binding site that would prevent it from binding and catalysis, without relevant impact in the recognition of ATP.

In contrast, the results of the MD simulations with the G5K enzyme complexes resulted from the addition of the substrates to the **50**@G5K binary complex indicated that both compounds (inhibitor **54** and L-Glu) are stable in their corresponding pockets during the simulation. However, significant differences were observed at the ATP binding site, which is spatially closer to the inhibitor binding site (Fig. 9B). Thus, the binding of inhibitor **50** triggers an alternative folding of the enzyme region that fixes the adenosine moiety of ATP in the active site, specifically residues 194–214 (*Ec*-G5K) and 211–221 (*Mt*-G5K) which contains the residues H215 (*Mt*-G5K), and I201 (*Ec*-G5K). An opening of up to 11.6 Å is observed. This is also visualized by the analysis of the most relevant contacts of the adenosine group during the simulation. For the *E. coli* enzyme, the average distance between the N6 atom in ATP and oxygen atom of the main carbonyl group in I201 was increased from 3.2 Å in the Michaelis complex to 8.2 Å in presence of inhibitor **50**, and the interaction between the hydroxyl group (O2

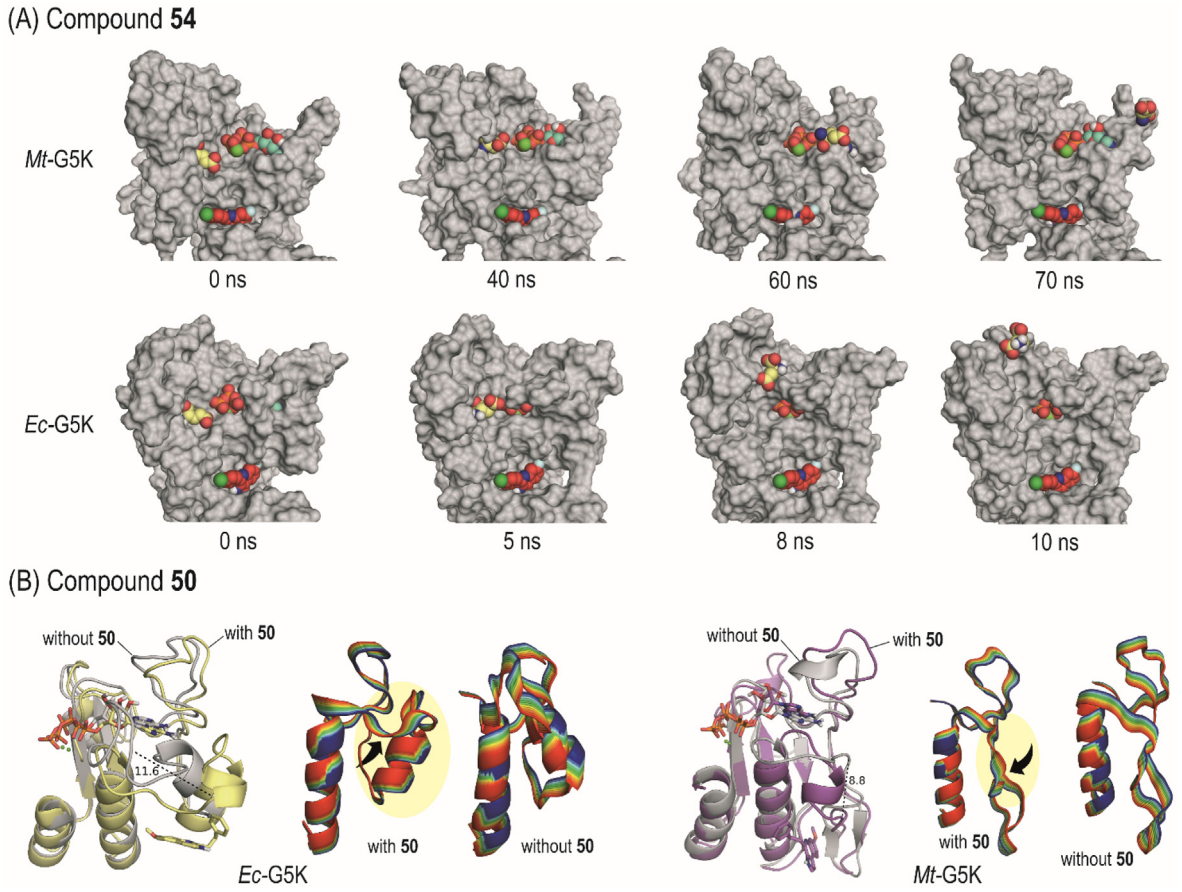

Fig. 9. Impact of the allosteric interaction of compounds **54** (A) and **50** (B) on the ability of the G5K enzymes to bind the natural substrates obtained by MD simulation studies. (A) Snapshots from the 100 ns MD simulation of the enzyme complex resulted from the addition of substrates (Glu, ATP-Mg^{2+}) to the **54**@G5K binary complex. Note how compound **54** (red) and ATP-Mg^{2+} (blue) are stable in the enzyme pocket during the simulation, whereas glutamate (yellow) is expelled from the catalytic site. (B) Comparison of the enzyme arrangement obtained after 100 ns of simulation of the enzyme complex resulted from the addition of ATP-Mg^{2+} to the **50**@G5K binary complex and the Michaelis complex. Detailed view of the motion of the ATP binding site in both complexes obtained by examination of the vibrational modes are also shown. Note the more reduced flexibility of the ATP recognition pocket in the **50**@G5K binary complex and the more open conformation of this enzyme region induced by **50**. Displacement of up to 11.6 Å are observed (black dashed lines). Hydrogen-bonding and electrostatic interactions are indicated as red dashed lines. Mg^{2+} is shown as a green sphere.

atom) in ATP and the carboxylate group (OD1 and OD2 atoms) in D178 also grew from 3.0 Å to 3.5 Å (OD2 atom) and from 4.1 Å to 4.8 Å (OD1 atom) (Fig. S6 *vs* S8). For the *M. tuberculosis* enzyme, a similar scenario was observed. Thus, the average distance between the N7 atom in ATP and: (i) the nitrogen atom of the main carbonyl group in T218; and (ii) the NE2 atom of the side chain in H215; was increased from 4.1 Å and 5.3 Å in the Michaelis complex to 9.1 Å and 14.9 Å, respectively, in the presence of **50** (Fig. S7 *vs* S8). The same occurred with the contact between the hydroxyl group (O2 atom) in ATP and the carboxylate group (OD1 and OD2 atoms) in D178 that changed from 3.0 Å to 3.5 Å (OD2 atom) and from 4.1 Å to 4.8 Å (OD1 atom). Furthermore, an examination of the vibrational modes for the **50**@G5K binary complexes and those resulting from adding the natural substrates to the above, calculated by PCA (principal component analysis), as implemented in AMBER, also showed a significant reduction on the intrinsic shape-motion of the aforementioned enzyme regions compared with the Michaelis complexes (Fig. 9B). The binding free energies of ATP in these complexes were calculated using the MM/PBSA approach in explicit water (generalized Born, GB) as implemented in Amber (Table 3). The results revealed the significant lost of affinity of ATP for the enzyme upon compound **50** binding, with calculated binding energy differences over 100 kcal mol^{-1}, which agrees with the experimentally observed increase in the K_m^{app} for ATP caused by this inhibitor. Taken together, these outcomes suggest that the inhibitory capacity of compound **50** against G5K could arise due to the long-distance conformational changes caused in the ATP binding site, which destabilize the binding of ATP for catalysis.

3. Conclusions

Chemical modification of positions 1, 3, 4 and 7 of the Marinoquinoline scaffold has led to the discovery of two new pyrroloquinolines (compounds **50** and **54**) with good *in vitro* activity against virulent strains of *M. tuberculosis* (H37Rv). These compounds, which were found to have MIC values of 4.1 and 4.2 μM,

Table 3
Calculated binding free energies (kcal mol^{-1}) of ATP in several enzyme complexes using MM/GBSA method.[a].

Enzyme complex	Energy	Relative Energy Difference
ATP-Mg^{2+}@*Mt*-G5K	−238.0 ± 0.5[b]	0
50+ATP-Mg^{2+}@*Mt*-G5K	−126.7 ± 0.5[b]	+111.3
Glu + ATP-Mg^{2+}@*Ec*-G5K	−232.3 ± 0.8[b]	0
50 + Glu + ATP-Mg^{2+}@*Ec*-G5K	−127.5 ± 0.4[b]	+104.8

[a] Only the last 80 ns of the whole simulation were considered for the calculations.
[b] Standard error of mean.

respectively, were synthesized in three steps from commercially available 3-(4,4,5,5-tetramethyl [1–3]dioxaborolan-2-yl)-1-(triisopropylsilanyl)-1*H*-pyrrole (**65**) in a reaction involving a Suzuki–Miyaura cross-coupling reaction and cyclization as key steps.

The reported compounds showed to be allosteric inhibitors of glutamate-5-kinase (G5K), which is an essential enzyme for this pathogen involved in the proline biosynthesis pathway, as demonstrated by the inhibition assays carried out with the isolated enzyme. Both compounds **50** and **54** were also found not to compete with L-Pro, which is the natural inhibitor.

The results of the MD simulation studies carried out for the ligand@G5K enzyme complexes revealed that compounds **50** and **54** bind at the interface between enzyme domains, but in different pockets and with different recognition patterns. Specifically, compound **54** would bind in the allosteric pocket close to the L-Glu catalytic site, while inhibitor **50** would target the pocket nearby to the ATP adenosine group recognition pocket. The computational studies performed with the Michaelis complexes of G5K, as well as the those resulted from the addition of substrates (L-Glu, ATP-Mg^{2+}) to ligand@G5K showed that the inhibitory capacity of compound **50** may arise due to long-distance conformational changes caused in the ATP binding site that hinder the binding of ATP for catalysis. The latter is in accordance with the enzyme assays results revealing that the binding of compound **50** causes the increase of the K_m^{app} for ATP. In contrast, the allosteric inhibition of compound **54** appears to be caused by conformational changes in the L-Glu catalytic site, avoiding the anchoring of L-Glu for catalysis. In contrast to compound **50**, the allosteric binding of **54** showed to cause no significant effect on the ATP recognition, as found in enzyme assays and *in silico* studies. The results of the studies described herein have allowed us to identify two promising scaffolds for the design of allosteric inhibitors of the G5K enzyme and reinforce the therapeutic potential of this biological target for the development of new anti-TB drugs.

4. Experimental

4.1. General methods

All starting materials and reagents were commercially available and were used without further purification. Column chromatography was generally performed using silica gel (230–400 mesh). Thin layer chromatography was performed employing Merck® Silica gel 60 F254 plates, using UV fluorescence and/or staining with: vanillin in methanolic sulfuric acid and cerium sulfate in aqueous sulfuric acid. ^{1}H NMR spectra (300 and 500 MHz), ^{13}C NMR spectra (75 and 125 MHz), and ^{19}F NMR spectra (282 MHz) were measured in deuterated solvents. *J* values are given in hertz. NMR assignments were carried out by a combination of 1 D, and DEPT-135 experiments. Melting points were measured in a Büchi M – 560 apparatus. Electrospray (ESI) mass spectra were recorded on a Bruker BIOTOF II mass spectrometer. The purity of the reported compounds was analyzed by HPLC and by NMR. HPLC was performed on a Thermo Dionex UltiMate 3000 apparatus having a Brucker amazon SL mass spectrometry detector, using a Phenomenex kinetex XB-C18 column (particle size = 1.7 μm; dimensions: 50 mm × 2.1 mm, pore size = 100 Å), and eluting at a flow rate of 0.35 mL min^{-1} with a gradient of 5–75% B in 10 min [A = Milli-Q water + 0.1% TFA; B = acetonitrile + 0.1% TFA]. All tested compounds have a purity ≥95%. The HPLC traces and NMR spectra are included in the supporting information. Compounds **8**–**40** were prepared as previously reported [29].

4.2. General Suzuki-Miyaura cross-coupling procedure for the preparation of compounds **66**–**71**

A suspension of $Pd(OAc)_2$ (43 mg, 0.19 mmol), SPhos (157 mg, 0.38 mmol), K_3PO_4 (2 g, 9.54 mmol), 3-(4,4,5,5-tetramethyl-1,3,2-dioxaborolan-2-yl)-1-(triisopropylsilyl)-1*H*-pyrrole (**65**) [30,36] (2 g, 5.79 mmol), and the corresponding bromoanilines (5.26 mmol), in a mixture of *n*-BuOH (6.8 mL) and water (2.7 mL) was heated at 80 °C for 12 h. After cooling to room temperature, the reaction mixture was diluted with water and ethyl acetate. The organic layer was separated, and the aqueous layer was extracted with ethyl acetate (× 2, 20 mL). The combined organic extracts were washed with brine, dried (anh. Na_2SO_4), filtered and concentrated under reduced pressure. The crude product was purified by flash chromatography to give the corresponding aryl pyrroles **66**–**71**.

4.2.1. 2-(1-(Triisopropylsilyl)-1H-pyrrol-3-yl)aniline (**66**, G = H)

It was prepared using the general Suzuki-Miyaura cross-coupling procedure and 2-bromoaniline. Eluent for chromatography: gradient of ethyl acetate/hexane 1) (3:97); 2) (5:95). R_f = 0.42 [(5:95) ethyl acetate/hexane]. Yield = 1.53 g (93%). Yellow oil. The spectroscopic data agreed with previously described [29]. ^{1}H NMR (300 MHz, $CDCl_3$) δ: 7.25 (dd, *J* = 7.5 and 1.4 Hz, 1H, CH), 7.03 (td, *J* = 7.7 and 1.5 Hz, 1H, CH), 6.96 (dd, *J* = 2.0 and 2.0 Hz, 1H, CH), 6.85 (dd, *J* = 2.4 and 2.4 Hz, 1H, CH), 6.78 (dd, *J* = 7.6 and 1.6 Hz, 1H, CH), 6.72 (dd, *J* = 7.6 and 1.6 Hz, 1H, CH), 6.51 (dd, *J* = 2.5 and 1.4 Hz, 1H, CH), 3.86 (br s, 2H, NH_2), 1.47 (sept, *J* = 7.5 Hz, 3H, 3 × CH), and 1.12 (d, *J* = 7.5 Hz, 18H, 6 × CH_3) ppm. MS (ESI) *m*/*z* = 315 (MH^+). HRMS calcd for $C_{19}H_{31}N_2Si$ (MH^+): 315.2251; found, 315.2252.

4.2.2. 5-(Trifluoromethyl)-2-(1-(triisopropylsilyl)-1H-pyrrol-3-yl) aniline (**67**, G = CF_3)

It was prepared using the general Suzuki-Miyaura cross-coupling procedure and 2-bromo-5-(trifluoromethyl)aniline. Eluent for chromatography: gradient of ethyl acetate/hexane 1) (3:97); 2) (5:95). R_f = 0.47 [(5:95) ethyl acetate/hexane]. Yield = 1.40 g (71%). Orange oil. ^{1}H NMR (300 MHz, $CDCl_3$) δ: 7.32 (d, *J* = 7.8 Hz, 1H, CH), 7.01 (dd, *J* = 8.4 and *J* = 2.4 Hz, 1H, CH), 6.99 (t, *J* = 2.4 Hz, 1H, CH), 6.96 (d, *J* = 1.3 Hz, 1H, CH), 6.87 (dd, *J* = 8.2 and *J* = 2.1 Hz, 1H, CH), 6.52 (dd, *J* = 2.7 and *J* = 1.4 Hz, 1H, CH), 4.12 (br s, 3H, NH_2), 1.50 (sept, *J* = 7.5 Hz, 3H, 3 × CH), and 1.14 (d, *J* = 7.5 Hz, 18H, 6 × CH_3) ppm. ^{13}C NMR (75 MHz, $CDCl_3$) δ: 143.8 (C), 129.8 (CH), 128.8 (q, J_{C-F} = 32 Hz, C), 124.4 (q, J_{C-F} = 270 Hz, C), 125.8 (C), 125.2 (CH), 122.8 (C), 122.7 (CH), 115.0 (CH), 111.8 (CH), 110.5 (CH), 17.8 (6 × CH_3), and 11.7 (3 × CH) ppm. ^{19}F NMR (282 MHz, $CDCl_3$) δ: 62.6 (s, 3F, CF_3) ppm. MS (ESI) *m*/*z* = 383 (MH^+). HRMS calcd for $C_{20}H_{30}F_3N_2Si$ (MH^+): 383.2125; found, 383.2125.

4.2.3. 5-Fluoro-2-(1-(triisopropylsilyl)-1H-pyrrol-3-yl)aniline (**68**, G = F)

It was prepared using the general Suzuki-Miyaura cross-coupling procedure and 2-bromo-5-fluoroaniline. Eluent for chromatography: gradient of ethyl acetate/hexane 1) (3:97); 2) (5:95). R_f = 0.58 [(5:95) ethyl acetate/hexane]. Yield = 1.52 g (87%). Pale orange oil. ^{1}H NMR (300 MHz, $CDCl_3$) δ: 7.16 (t, *J* = 2.4 Hz, 1H, CH), 6.89 (t, *J* = 1.7 Hz, 1H, CH), 6.85 (t, *J* = 2.4 Hz, 1H, CH), 6.50–6.43 (m, 3H, 3 × CH), 4.05 (s, 2H, NH_2), 1.48 (sept, *J* = 7.5 Hz, 3H, 3 × CH), 1.14 (d, *J* = 7.5 Hz, 18H, 6 × CH_3) ppm. ^{13}C NMR (75 MHz, $CDCl_3$) δ: 162.4 (d, J_{C-F} = 242 Hz, C), 145.3 (d, J_{C-F} = 11 Hz, C), 130.9 (d, J_{C-F} = 10 Hz, CH), 125.0 (CH), 123.1 (C), 122.3 (CH), 118.6 (C), 110.8 (CH), 105.0 (d, J_{C-F} = 21 Hz, CH), 102.0 (d, J_{C-F} = 24 Hz, CH), and 18.0 (6 × CH_3), and

11.79 (3 × CH) ppm. ^{19}F NMR (282 MHz, $CDCl_3$) δ: 116.4 (q, J = 7.6 Hz, 1F, CF) ppm. MS (ESI) m/z = 333 (MH^+). HRMS calcd for $C_{19}H_{30}FN_2Si$ (MH^+): 333.2157; found, 333.2155.

4.2.4. 5-Chloro-2-(1-(triisopropylsilyl)-1H-pyrrol-3-yl)aniline (**69**, G = Cl)

It was prepared using the general Suzuki-Miyaura cross-coupling procedure and 2-bromo-5-chloroaniline. Eluent for chromatography: (5:95) ethyl acetate/hexane. R_f = 0.38 [(5:95) ethyl acetate/hexane]. Yield = 1.27 g (69%). Pale yellow solid. Mp: 65–66 °C. ^{1}H NMR (300 MHz, $CDCl_3$) δ: 7.16 (d, J = 8.1 Hz, 1H, CH), 6.93 (br s, 1H, CH), 6.83 (br s, 1H, CH), 6.78 (m, 2H, 2 × CH), 6.47 (m, 1H, CH), 3.98 (br s, 2H, NH_2), 1.45 (sept, J = 7.5 Hz, 3H, 3 × CH), and 1.12 (d, J = 7.4 Hz, 18H, 6 × CH_3) ppm. ^{13}C NMR (75 MHz, $CDCl_3$) δ: 144.9 (C), 132.2 (C), 130.8 (CH), 125.1 (CH), 123.0 (C), 122.4 (CH), 121.2 (C), 118.5 (CH), 115.1 (CH), 110.7 (CH), 18.0 (6 × CH_3), and 11.8 (3 × CH) ppm. MS (ESI) m/z = 349 (MH^+). HRMS calcd for $C_{19}H_{30}ClN_2Si$ (MH^+): 349.1861; found, 349.1862.

4.2.5. Methyl 3-amino-4-(1-(triisopropylsilyl)-1H-pyrrol-3-yl) benzoate (**70**, G = CO_2Me)

It was prepared using the general Suzuki-Miyaura cross-coupling procedure and methyl 3-amino-4-bromobenzoate. Eluent for chromatography: gradient of ethyl acetate/hexane 1) (5:95); 2) (15:85). R_f = 0.36 [(5:95) ethyl acetate/hexane]. Yield = 1.32 g (68%). Pale yellow solid. Mp: 96–97 °C. ^{1}H NMR (300 MHz, $CDCl_3$) δ: 7.46 (dd, J = 8.4 and J = 2.6 Hz, 1H, CH), 7.44 (s, 1H, CH), 7.32 (d, J = 8.5 Hz, 1H, CH), 7.04 (t, J = 1.6 Hz, 1H, CH), 6.87 (t, J = 2.4 Hz, 1H, CH), 6.55 (dd, J = 2.5 and J = 1.5 Hz, 1H, CH), 4.04 (br s, 2H, NH_2), 3.88 (s, 3H, CH_3), 1.48 (sept, J = 7.5 Hz, 3H, 3 × CH), and 1.14 (d, J = 7.5 Hz, 18H, 6 × CH_3) ppm. ^{13}C NMR (75 MHz, $CDCl_3$) δ: 167.4 (C), 143.6 (C), 129.3 (CH), 128.2 (C), 127.3 (C), 125.2 (CH), 123.3 (C), 122.8 (CH), 119.9 (CH), 116.5 (CH), 110.6 (CH), 51.9 (CH), 17.9 (6 × CH_3), and 11.7 (3 × CH) ppm. MS (ESI) m/z = 373 (MH^+). HRMS calcd for $C_{21}H_{33}N_2O_2Si$ (MH^+): 373.2306; found, 373.2306.

4.2.6. 5-Methyl-2-(1-(triisopropylsilyl)-1H-pyrrol-3-yl)aniline (**71**, G = Me)

It was prepared using the general Suzuki-Miyaura cross-coupling procedure and 2-bromo-5-methylaniline. Eluent for chromatography: gradient of ethyl acetate/hexane 1) (3:97); 2) (6:94). R_f = 0.38 [(5:95) ethyl acetate/hexane]. Yield = 1.54 g (92%). Orange oil. ^{1}H NMR (300 MHz, $CDCl_3$) δ: 7.23 (d, J = 8.1 Hz, 1H, CH), 7.01 (s, 1H, CH), 6.91 (dd, J = 8.6 and J = 2.6 Hz, 1H, CH), 6.68 (d, J = 6.8, 1H, CH), 6.61 (s, 1H, CH), 6.48 (dd, J = 2.5 and J = 1.3 Hz, 1H, CH), 3.87 (br s, 2H, NH_2), 2.29 (s, 3H, CH_3), 1.55 (sept, J = 7.5 Hz, 3H, 3 × CH), and 1.21 (d, J = 7.5 Hz, 18H, 6 × CH_3) ppm. ^{13}C NMR (75 MHz, $CDCl_3$) δ: 143.6 (C), 136.7 (C), 129.6 (CH), 124.6 (CH), 123.9 (C), 122.2 (CH), 119.9 (C), 119.5 (CH), 116.2 (CH), 110.9 (CH), 21.2 (CH_3), 17.9 (6 × CH_3), and 11.8 (3 × CH) ppm. MS (ESI) m/z = 329 (MH^+). HRMS calcd for $C_{20}H_{33}N_2Si$ (MH^+): 329.2408; found, 329.2406.

4.3. Preparation of compounds **72**–**77**

4.3.1. 2-(1H-pyrrol-3-yl)aniline (**72**, G = H)

A solution of compound **66** (1.46 g, 4.64 mmol) in dry THF (4.6 mL), under argon and at room temperature, was treated with tetrabutylammonium fluoride (5.1 mL, 5.10 mmol, *ca* 1 M in THF). The resultant mixture was stirred for 15 min. Water and dichloromethane were added, the organic layer was separated and the aqueous layer was extracted with dichloromethane (× 2). The combined organic extracts were washed with brine, dried (anh. Na_2SO_4), filtered and concentrated under reduced pressure. The resulting residue was purified by flash chromatography, eluting with a gradient of ethyl acetate/hexane: 1) (20:80); 2) (50:50), to give the compound **72** (646 mg, 89%), as a pale yellow oil. R_f = 0.39 [(30:70) ethyl acetate/hexane]. The spectroscopic data agreed with previously described [29]. ^{1}H NMR (300 MHz, $CDCl_3$) δ: 8.35 (br s, 1H, NH), 7.25 (d, J = 6.9 Hz, 1H, CH), 7.06 (t, J = 7.0 Hz, 1H, CH), 6.80 (d, J = 7.9 Hz, 2H, 2 × CH), 6.69 (d, J = 8.1 Hz, 2H, 2 × CH), 6.38 (s, 1H, CH), and 3.82 (s, 2H, NH_2) ppm. MS (ESI) m/z = 159 (MH^+). HRMS calcd for $C_{10}H_{11}N_2$ (MH^+): 159.0917; found, 159.0917.

4.3.2. 2-(1H-pyrrol-3-yl)-5-(trifluoromethyl)aniline (**73**, G = CF_3)

It was prepared according to the procedure described for compound **72** using: ether **67** (1.10 g, 2.87 mmol), tetrabutylammonium fluoride (3.16 mL, 3.16 mmol, *ca* 1 M in THF). Eluent for chromatography: (30:70) ethyl acetate/hexane. R_f = 0.50 [(30:70) ethyl acetate/hexane]. Yield = 604 mg (93%). White solid. Mp: 92–93 °C. ^{1}H NMR (300 MHz, $CDCl_3$) δ: 8.43 (br s, 1H, NH), 7.34 (d, J = 7.9 Hz, 1H, CH), 7.07–6.96 (m, 3H, 3 × CH), 6.90 (dd, J = 4.7 and J = 2.6 Hz, 1H, CH), 6.48 (dd, J = 4.2 and J = 2.6 Hz, 1H, CH), and 4.13 (s, 2H, NH_2) ppm. ^{13}C NMR (75 MHz, $CDCl_3$) δ: 144.1 (C), 130.1 (CH), 128.8 (q, J_{C-F} = 32 Hz, C), 124.4 (q, J_{C-F} = 270 Hz, C), 125.6 (C), 119.0 (CH), 120.9 (C), 116.7 (CH), 115.1 (CH), 111.9 (CH), and 108.6 (CH) ppm. ^{19}F NMR (282 MHz, $CDCl_3$) δ: 62.5 (s, 3F, CF_3) ppm. MS (ESI) m/z = 227 (MH^+). HRMS calcd for $C_{11}H_{10}F_3N_2$ (MH^+): 227.0791; found, 227.0791.

4.3.3. 5-Fluoro-2-(1H-pyrrol-3-yl)aniline (**74**, G = F)

It was prepared according to the procedure described for compound **72** using: ether **68** (1.48 g, 4.45 mmol), tetrabutylammonium fluoride (4.9 mL, 4.90 mmol, *ca* 1 M in THF). Eluent for chromatography: (30:70) ethyl acetate/hexane. R_f = 0.47 [(30:70) ethyl acetate/hexane]. Yield = 768 mg (98%). White solid. Mp: 67–68 °C. ^{1}H NMR (300 MHz, $CDCl_3$) δ: 8.39 (br s, 1H, NH), 7.19 (dd, J = 8.1 and J = 6.7 Hz, 1H, CH), 6.92 (dd, J = 4.0 and J = 2.0 Hz, 1H, CH), 6.87 (dd, J = 4.5 and J = 2.3 Hz, 1H, CH), 6.55–6.44 (m, 2H, 2 × CH), 6.41 (dd, J = 4.1 and J = 2.3 Hz, 1H, CH), and 3.98 (br s, 2H, NH_2) ppm. ^{13}C NMR (75 MHz, $CDCl_3$) δ: 162.4 (d, J_{C-F} = 242 Hz, C), 145.4 (d, J_{C-F} = 11.0 Hz, C), 131.0 (d, J_{C-F} = 9.6 Hz, CH), 121.0 (C), 118.7 (CH), 118.3 (C), 116.1 (CH), 108.6 (CH), 105.0 (d, J_{C-F} = 21 Hz, CH), and 102.0 (d, J_{C-F} = 25 Hz, CH) ppm. ^{19}F NMR (282 MHz, $CDCl_3$) δ: 116.4 (s, 1F, CF) ppm. MS (ESI) m/z = 177 (MH^+). HRMS calcd for $C_{10}H_{10}FN_2$ (MH^+): 227.0791; found, 177.0823.

4.3.4. 5-Chloro-2-(1H-pyrrol-3-yl)aniline (**75**, G = cl)

It was prepared according to the procedure described for compound **72** using: ether **69** (1.19 g, 3.41 mmol), tetrabutylammonium fluoride (3.75 mL, 3.75 mmol, *ca* 1 M in THF). Eluent for chromatography: (30:70) ethyl acetate/hexane. R_f = 0.45 [(30:70) ethyl acetate/hexane]. Yield = 525 mg (80%). White solid. Mp: 93–94 °C. ^{1}H NMR (300 MHz, $CDCl_3$) δ: 8.37 (br s, 1H, NH), 7.14 (d, J = 8.7 Hz, 1H, CH), 6.98–6.93 (m, 1H, CH), 6.88 (dd, J = 4.8 and J = 2.5 Hz, 1H, CH), 6.77–6.72 (m, 2H, 2 × CH), 6.41 (dd, J = 4.1 and J = 2.3 Hz, 1H, CH), and 4.01 (br s, 2H, NH_2) ppm. ^{13}C NMR (75 MHz, $CDCl_3$) δ: 144.9 (C), 132.4 (C), 130.8 (CH), 120.9 (C),120.8 (C), 118.8 (CH), 118.4 (CH), 116.2 (CH), 115.1 (CH), and 108.5 (CH) ppm. MS (ESI) m/z = 193 (MH^+). HRMS calcd for $C_{10}H_{10}ClN_2$ (MH^+): 193.0527; found, 193.0526.

4.3.5. Methyl 3-amino-4-(1H-pyrrol-3-yl)benzoate (**76**, G = CO_2Me)

It was prepared according to the procedure described for compound **72** using: ether **70** (1.22 g, 3.30 mmol), tetrabutylammonium fluoride (3.60 mL, 3.60 mmol, *ca* 1 M in THF). Eluent for chromatography: (30:70) ethyl acetate/hexane. R_f = 0.54 [(30:70) ethyl acetate/hexane]. Yield = 634 mg (89%). Pale yellow solid. Mp: 117–118 °C. ^{1}H NMR (300 MHz, $CDCl_3$) δ: 8.65 (br s, 1H, NH), 7.46

(dd, J = 7.9 and 1.7 Hz, 1H, CH), 7.43 (d, J = 1.4 Hz, 1H, CH), 7.31 (d, J = 7.8 Hz, 1H, CH), 7.06 (dd, J = 4.2 and 1.8 Hz, 1H, CH), 6.89 (dd, J = 4.7 and 2.6 Hz, 1H, CH), 6.49 (dd, J = 4.2 and 2.6 Hz, 1H, CH), 4.15 (br s, 2H, NH_2), and 3.90 (s, 3H, CH_3) ppm. ^{13}C NMR (75 MHz, $CDCl_3$) δ: 167.6 (C), 143.7 (C), 129.5 (CH), 128.4 (C), 127.1 (C), 121.2 (C), 120.0 (CH), 119.0 (CH), 116.8 (CH), 116.5 (CH), 108.5 (CH), and 52.1 (s, CH_3) ppm. MS (ESI) m/z = 217 (MH^+). HRMS calcd for $C_{12}H_{13}N_2O_2$ (MH^+): 217.0972; found, 217.0972.

4.3.6. 5-Methyl-2-(1H-pyrrol-3-yl)aniline (**77**, G = Me)

It was prepared according to the procedure described for compound **72** using: ether **71** (1.54 g, 4.70 mmol), tetrabutylammonium fluoride (5.16 mL, 5.16 mmol, *ca* 1 M in THF). Eluent for chromatography: (30:70) ethyl acetate/hexane. R_f = 0.63 [(30:70) ethyl acetate/hexane]. Yield = 712 mg (88%). Pale yellow solid. Mp: 84–85 °C. ^{1}H NMR (300 MHz, $CDCl_3$) δ: 8.44 (br s, 1H, NH), 7.24 (d, J = 7.7 Hz, 1H, CH), 6.93 (dd, J = 7.9 and 1.7 Hz, 1H, CH), 6.85 (dd, J = 4.9 and 2.4 Hz, 1H, CH), 6.72 (dd, J = 7.6 and 1.5 Hz, 1H, CH), 6.67 (s, 1H, CH), 6.48 (dd, J = 4.2 and 2.6 Hz, 1H, CH), 3.90 (s, 2H, NH_2), and 2.37 (s, 3H, CH_3) ppm. ^{13}C NMR (75 MHz, $CDCl_3$) δ: 143.5 (C), 137.0 (C), 129.8 (CH), 121.6 (C), 119.6 (C + CH), 118.5 (CH), 116.4 (CH), 116.1 (CH), 108.5 (CH), and 21.2 (CH_3) ppm. MS (ESI) m/z = 173 (MH^+). HRMS calcd for $C_{11}H_{13}N_2$ (MH^+): 173.1073; found, 173.1074.

4.4. Preparation of compounds **42**–**50** and **52**–**57**

4.4.1. 4-n-Octyl-3H-pyrrolo [2,3-c]quinoline (**42**)

A solution of aniline **72** (100 mg, 0.63 mmol) and pelargonaldehyde (130 μL, 0.76 mmol) in dichloromethane (2 mL) at room temperature was treated with TFA (48 μL, 0.63 mmol) and stirred for 1 h. The solvent was then removed under reduced pressure. The resulting residue was basified with aq. $NaHCO_3$ and then extracted with ethyl acetate (3 ×). The combined organic extracts were washed with brine, dried (anh. Na_2SO_4), filtered and concentrated under reduced pressure. The crude was purified by flash chromatography, eluting with (30:70) ethyl acetate/hexane, to give compound **42** (103 mg, 58%), as a brown solid. R_f = 0.38 [(30:70) ethyl acetate/hexane]. Mp: 91–93 °C. ^{1}H NMR (500 MHz, $CDCl_3$) δ: 10.79 (br s, 1H, NH), 8.23–8.19 (m, 1H, CH), 8.18–8.13 (m, 1H, CH), 7.58–7.52 (m, 2H, CH), 7.50 (d, J = 3.0 Hz, 1H, CH), 7.10 (d, J = 3.0 Hz, 1H, CH), 3.06 (t, J = 8.0 Hz, 2H, CH_2), 1.73 (dt, J = 15.7 and J = 7.9 Hz, 2H, CH_2), 1.22–1.13 (m, 2H, CH_2), 1.05 (m, 8H, 4 × CH_2), and 0.82 (t, J = 7.3 Hz, 3H, CH_3) ppm. ^{13}C NMR (125 MHz, $CDCl_3$) δ: 150.3 (C), 142.4 (C), 128.8 (C), 128.4 (C), 128.3 (CH), 126.5 (CH), 126.1 (CH), 125.4 (CH), 123.2 (C), 123.2 (CH), 102.0 (CH), 35.2 (CH_2), 31.9 (CH_2), 29.9 (CH_2), 29.5 (2 × CH_2), 29.2 (CH_2), 22.7 (CH_2), and 14.2 (CH_3) ppm. MS (ESI) m/z = 281 (MH^+). HRMS calcd for $C_{19}H_{25}N_2$ (MH^+): 281.2012; found, 281.2014.

4.4.2. 7-Fluoro-4-n-octyl-3H-pyrrolo [2,3-c]quinoline (**43**)

It was prepared according to the procedure described for compound **42** using: aniline **74** (70 mg, 0.40 mmol), pelargonaldehyde (82 μL, 0.48 mmol). Eluent for chromatography: (15:85) ethyl acetate/hexane. R_f = 0.60 [(30:70) ethyl acetate/hexane]. Yield = 55 mg (46%). Pale yellow solid. Mp: 105–106 °C. ^{1}H NMR (300 MHz, $CDCl_3$) δ: 10.21 (br s, 1H, NH), 8.15 (dd, J = 8.6 and J = 6.3 Hz, 1H, CH), 7.78 (dd, J = 10.5 and J = 1.5 Hz, 1H, CH), 7.49 (d, J = 2.1 Hz, 1H, CH), 7.37–7.27 (m, 1H, CH), 7.05 (d, J = 2.5 Hz, 1H, CH), 3.08 (t, J = 8.0 Hz, 2H, CH_2), 1.77 (dt, J = 15.7 and J = 7.9 Hz, 2H, CH_2), 1.11 (m, 10H, 5 × CH_2), and 0.82 (t, J = 6.9 Hz, 3H, CH_3) ppm. ^{13}C NMR (75 MHz, $CDCl_3$) δ: 161.2 (d, J_{C-F} = 244 Hz, C–F), 151.2 (C), 143.4 (d, J_{C-F} = 12 Hz, C), 128.8 (C), 128.1 (C), 126.7 (CH), 124.7 (d, J_{C-F} = 10 Hz, CH), 119.9 (C), 114.9 (d, J_{C-F} = 24 Hz, CH), 112.8 (d, J_{C-F} = 21 Hz, CH), 101.9 (CH), 35.2 (CH_2), 31.9 (CH_2), 30.0 (CH_2), 29.5 (CH_2), 29.3 (CH_2), 29.3 (CH_2), 22.7 (CH_2), and 14.2 (CH_3) ppm. ^{19}F NMR (282 MHz, $CDCl_3$) δ: 115.5 (s, 1F, CF) ppm. MS (ESI) m/z = 299 (MH^+). HRMS calcd for $C_{19}H_{24}FN_2$ (MH^+): 299.1918; found, 299.1918.

4.4.3. 7-Methyl-4-n-octyl-3H-pyrrolo [2,3-c]quinoline (**44**)

It was prepared according to the procedure described for compound **42** using: aniline **77** (70 mg, 0.41 mmol), pelargonaldehyde (84 μL, 0.49 mmol). Eluent for chromatography: (30:70) ethyl acetate/hexane. R_f = 0.37 [(30:70) ethyl acetate/hexane]. Yield = 63 mg (52%). Pale brown solid. Mp: 111–112 °C. ^{1}H NMR (300 MHz, $CDCl_3$) δ: 10.70 (br s, 1H, NH), 8.10 (d, J = 8.2 Hz, 1H, CH), 7.95 (s, 1H, CH), 7.48 (d, J = 2.9 Hz, 1H, CH), 7.38 (d, J = 8.2 Hz, 1H, CH), 7.05 (d, J = 2.9 Hz, 1H, CH), 3.08–2.94 (m, 2H, CH_2), 2.53 (s, 3H, CH_3), 1.71 (s, 2H, CH_2), 1.26–0.97 (m, 10H, 5 × CH_2), and 0.82 (t, J = 7.1 Hz, 3H, CH_3) ppm. ^{13}C NMR (125 MHz, $CDCl_3$) δ: 150.2 (C), 142.7 (C), 135.8 (C), 128.7 (C), 128.2 (C), 127.9 (CH), 127.3 (CH), 126.3 (CH), 122.9 (CH), 120.9 (C), 101.7 (CH), 35.2 (CH_2), 31.9 (CH_2), 29.9 (CH_2), 29.5 (CH_2), 29.5 (CH_2), 29.3 (CH_2), 22.7 (CH_2), 21.8 (CH_3), and 14.2 (CH_3) ppm. MS (ESI) m/z = 295 (MH^+). HRMS calcd for $C_{20}H_{27}N_2$ (MH^+): 295.2168; found, 295.2172.

4.4.4. 7-Methoxy-4-n-octyl-3H-pyrrolo [2,3-c]quinoline (**45**)

It was prepared according to the procedure described for compound **42** using: 5-methoxy-2-(1*H*-pyrrol-3-yl)aniline (**78**) [29] (70 mg, 0.37 mmol), pelargonaldehyde (77 μL, 0.45 mmol). Eluent for chromatography: (40:60) ethyl acetate/hexane. R_f = 0.51 [(50:50) ethyl acetate/hexane]. Yield = 41 mg (36%). Brown oil. ^{1}H NMR (300 MHz, $CDCl_3$) δ: 9.42 (s, 1H, NH), 8.06 (d, J = 8.9 Hz, 1H, ArH), 7.55 (d, J = 2.5 Hz, 1H, ArH), 7.41 (d, J = 3.0 Hz, 1H, ArH), 7.20 (dd, J = 2.6 and 8.9 Hz, 1H, ArH), 6.99 (d, J = 3.0 Hz, 1H, ArH), 3.91 (s, 3H, OCH_3), 3.11 (t, J = 8.0 Hz, 2H, CH_2), 1.86 (q, J = 7.7 Hz, 2H, CH_2), 1.37–1.19 (m, 10H, 5 × CH_2) and 0.84 (t, J = 6.8 Hz, 3H, CH3) ppm. ^{13}C NMR (75 MHz, $CDCl_3$) δ: 158.3 (C), 150.1 (C), 144.0 (C), 129.0 (C), 127.7 (C), 126.3 (CH), 124.1 (CH), 117.5 (C), 117.1 (CH), 108.3 (CH), 101.5 (CH), 55.5 (OCH3), 35.4 (CH_2), 31.9 (CH_2), 30.0 (CH_2), 29.6 (CH_2), 29.4 (CH_2), 29.3 (CH_2), 22.7 (CH_2) and 14.2 (CH_3) ppm. MS (ESI) m/z = 293 (MH^+). HRMS calcd for $C_{20}H_{27}N_2O$ (MH^+): 311.2118; found, 311.2118.

4.4.5. 4-Cyclopropyl-3H-pyrrolo [2,3-c]quinoline (**46**)

It was prepared according to the procedure described for compound **42** using: aniline **72** (100 mg, 0.63 mmol), cyclopropanecarbaldehyde (57 μL, 0.76 mmol). Eluent for chromatography: (30:70) ethyl acetate/hexane. R_f = 0.40 [(30:70) ethyl acetate/hexane]. Yield = 92 mg (70%). Brown solid. Mp: 130–132 °C. ^{1}H NMR (500 MHz, $CDCl_3$) δ: 9.26 (br s, 1H, NH), 8.15 (dd, J = 7.8 and J = 1.5 Hz, 1H, CH), 8.09 (d, J = 8.0 Hz, 1H, CH), 7.52 (m, 1H, 2 × CH), 7.43 (d, J = 3.0 Hz, 1H, CH), 7.07 (d, J = 2.9 Hz, 1H, CH), 2.37 (m, 1H, CH), 1.43–1.38 (m, 1H, CH_2), and 1.12–1.07 (m, 1H, CH_2) ppm. ^{13}C NMR (125 MHz, $CDCl_3$) δ: 149.5 (C), 142.5 (C), 128.9 (C), 128.7 (CH), 127.7 (C), 125.9 (CH), 125.6 (CH), 125.0 (CH), 122.8 (CH), 122.8 (C), 102.1 (CH), 13.5 (CH), and 8.1 (2 × CH_2) ppm. MS (ESI) m/z = 281 (MH^+). HRMS calcd for $C_{14}H_{13}N_2$ (MH^+): 209.1073; found, 209.1074.

4.4.6. 4-Cyclopropyl-7-methyl-3H-pyrrolo [2,3-c]quinoline (**47**)

It was prepared according to the procedure described for compound **42** using: aniline **77** (70 mg, 0.41 mmol), cyclopropanecarbaldehyde (36 μL, 0.49 mmol). Eluent for chromatography: (40:60) ethyl acetate/hexane. R_f = 0.35 [(30:70) ethyl acetate/hexane]. Yield = 51 mg (57%). Pale brown solid. Mp: 127–129 °C. ^{1}H NMR (300 MHz, $CDCl_3$) δ: 9.51 (br s, 1H, NH), 8.05 (d, J = 8.2 Hz, 1H, CH), 7.89 (s, 1H, CH), 7.42–7.29 (m, 2H, CH), 7.02 (d, J = 2.9 Hz, 1H, CH), 2.52 (s, 3H, CH_3), 2.29–2.19 (m, 1H, CH), 1.37–1.29 (m, 2H, CH_2), and 0.97 (m, 2H, CH_2) ppm. ^{13}C NMR

(75 MHz, $CDCl_3$) δ: 149.6 (C), 142.9 (C), 135.6 (C), 128.8 (C), 128.2 (CH), 127.6 (C), 126.8 (CH), 125.6 (CH), 122.6 (CH), 120.6 (C), 101.6 (CH), 21.6 (CH_3), 13.5 (CH), and 8.0 (2 × CH_2) ppm. MS (ESI) *m/z* = 223 (MH^+). HRMS calcd for $C_{15}H_{15}N_2$ (MH^+): 223.1229; found, 223.1229.

*4.4.7. 4-Phenethyl-3H-pyrrolo [2,3-c]quinoline (**48**)*

It was prepared according to the procedure described for compound **42** using: aniline **72** (50 mg, 0.32 mmol), hydrocinnamaldehyde (50 μL, 0.38 mmol). Eluent for chromatography: (40:60) ethyl acetate/hexane. R_f = 0.51 [(40:60) ethyl acetate/hexane]. Yield = 43 mg (50%). Brown solid. Mp: 135–136 °C. ^{1}H NMR (300 MHz, $CDCl_3$) δ: 8.83 (br s, 1H, NH), 8.22–8.15 (m, 2H, 2 × CH), 7.64–7.51 (m, 2H, 2 × CH), 7.28–7.07 (m, 6H, 6 × CH), 7.03 (d, *J* = 2.6 Hz, 1H, CH), 3.43 (t, *J* = 7.8 Hz, 2H, CH_2), and 3.23 (t, *J* = 7.7 Hz, 2H, CH_2) ppm. ^{13}C NMR (125 MHz, $CDCl_3$) δ: 148.7 (C), 148.6 (C), 142.8 (C), 141.8 (C), 141.8 (C), 128.9 (CH), 128.7 (2 × CH), 128.6 (C), 128.5 (2 × CH), 126.3 (CH), 126.2 (CH), 125.6 (CH), 123.2 (C), 123.1 (CH), 101.9 (CH), 37.2 (CH_2), and 35.1 (CH_2) ppm. MS (ESI) *m/z* = 273 (MH^+). HRMS calcd for $C_{19}H_{17}N_2$ (MH^+): 273.1386; found, 273.1385.

*4.4.8. 7-Fluoro-4-phenethyl-3H-pyrrolo [2,3-c]quinoline (**49**)*

It was prepared according to the procedure described for compound **42** using: aniline **74** (50 mg, 0.28 mmol), hydrocinnamaldehyde (45 μL, 0.34 mmol). Eluent for chromatography: (30:70) ethyl acetate/hexane. R_f = 0.41 [(40:60) ethyl acetate/hexane]. Yield = 29 mg (35%). Yellow solid. Mp: 129–131 °C. ^{1}H NMR (300 MHz, $CDCl_3$) δ: 8.67 (br s, 1H, NH), 8.15 (dd, *J* = 8.9 and *J* = 6.1 Hz, 1H, CH), 7.83 (dd, *J* = 10.7 and *J* = 2.5 Hz, 1H, CH), 7.34 (td, *J* = 8.7 and *J* = 2.6 Hz, 1H, CH), 7.30–7.26 (m, 1H, CH), 7.25–7.18 (m, 3H, 3 × CH), 7.14 (d, *J* = 7.6 Hz, 2H, 2 × CH), 6.99 (d, *J* = 2.9 Hz, 1H, CH), 3.44 (t, *J* = 7.7 Hz, 2H, CH_2), and 3.25 (t, *J* = 7.7 Hz, 2H, CH_2) ppm. ^{13}C NMR (125 MHz, $CDCl_3$) δ: 161.1 (d, $J_{C\text{-}F}$ = 244 Hz, C), 149.4 (C), 143.6 (d, $J_{C\text{-}F}$ = *J* = 12 Hz, C), 141.7 (C), 128.6 (2 × CH), 128.4 (2 × CH), 128.4 (C), 128.1 (C), 126.2 (2 × CH), 124.4 (d, $J_{C\text{-}F}$ = 10 Hz, CH), 119.7 (C), 114.8 (d, $J_{C\text{-}F}$ = 24 Hz, CH), 113.0 (d, $J_{C\text{-}F}$ = 20 Hz, CH), 101.7 (CH), 37.0 (CH_2), and 34.7 (CH_2) ppm. ^{19}F NMR (282 MHz, $CDCl_3$) δ: 115.5 (s, 1F, CF) ppm. MS (ESI) *m/z* = 291 (MH^+). HRMS calcd for $C_{19}H_{16}FN_2$ (MH^+): 291.1292; found, 291.1291.

*4.4.9. 7-Methoxy-4-phenethyl-3H-pyrrolo [2,3-c]quinoline (**50**)*

It was prepared according to the procedure described for compound **42** using: 5-methoxy-2-(1*H*-pyrrol-3-yl)aniline (**78**) [29] (100 mg, 0.53 mmol), hydrocinnamaldehyde (84 μL, 0.64 mmol). Eluent for chromatography: (50:50) ethyl acetate/hexane. R_f = 0.43 [(50:50) ethyl acetate/hexane]. Yield = 54 mg (34%). Pale yellow solid. Mp: 167–168 °C. ^{1}H NMR (500 MHz, $CDCl_3$) δ: 8.52 (br s, 1H, NH), 8.06 (d, *J* = 8.8 Hz, 1H, CH), 7.58 (d, *J* = 2.6 Hz, 1H, CH), 7.25–7.18 (m, 5H, 5 × CH), 7.14 (d, *J* = 6.8 Hz, 2H, 2 × CH), 6.94 (d, *J* = 3.0 Hz, 1H, CH), 3.95 (s, 3H, CH_3), 3.42 (t, *J* = 7.8 Hz, 2H, CH_2), and 3.24 (t, *J* = 7.8 Hz, 2H, CH_2) ppm. ^{13}C NMR (125 MHz, $CDCl_3$) δ: 158.2 (C), 148.4 (C), 144.1 (C), 141.8 (C), 128.7 (C), 128.6 (2 × CH), 128.4 (2 × CH), 127.8 (C), 126.2 (CH), 126.1 (CH), 124.0 (CH), 117.4 (C), 117.3 (CH), 108.3 (CH), 101.3 (CH), 55.5 (CH_3), 37.2 (CH_2), and 35.1 (CH_2) ppm. MS (ESI) *m/z* = 303 (MH^+). HRMS calcd for $C_{20}H_{19}N_2O$ (MH^+): 303.1492; found, 303.1489.

*4.4.10. 4-([1,1′-biphenyl]-4-yl)-3H-pyrrolo [2,3-c]quinoline (**52**)*

It was prepared according to the procedure described for compound **42** using: aniline **72** (50 mg, 0.32 mmol), [1,1′-biphenyl]-4-carbaldehyde (69 mg, 0.38 mmol). Eluent for chromatography: (30:70) ethyl acetate/hexane. R_f = 0.46 [(30:70) ethyl acetate/hexane]. Yield = 44 mg (43%). White solid. Mp: 172–175 °C. ^{1}H NMR (300 MHz, $CDCl_3$) δ: 9.43 (br s, 1H, NH), 8.27–8.22 (m, 2H, 2 × CH), 7.96 (d, *J* = 8.2 Hz, 2H, 2 × CH), 7.67 (d, *J* = 8.1 Hz, 2H, 2 × CH), 7.64–7.54 (m, 4H, 4 × CH), 7.49–7.43 (m, 3H, 3 × CH), 7.41–7.35 (m, 1H, CH), and 7.15–7.12 (m, 1H, CH) ppm. ^{13}C NMR (75 MHz, $CDCl_3$) δ: 146.5 (C), 143.0 (C), 142.0 (C), 140.4 (C), 137.2 (C), 129.7 (CH), 129.3 (C), 128.9 (2 × CH), 128.7 (2 × CH), 127.8 (2 × CH), 127.7 (CH), 127.5 (C), 127.1 (2 × CH), 126.4 (CH), 126.3 (CH), 125.9 (C), 123.2 (CH), 122.9 (CH), and 102.1 (CH) ppm. MS (ESI) *m/z* = 321 (MH^+). HRMS calcd for $C_{23}H_{17}N_2$ (MH^+): 321.1386; found, 321.1387.

*4.4.11. 4-(4-Chlorophenyl)-7-(trifluoromethyl)-3H-pyrrolo [2,3-c] quinoline (**53**)*

It was prepared according to the procedure described for compound **42** using: aniline **73** (70 mg, 0.31 mmol), 4-chlorobenzaldehyde (52 mg, 0.37 mmol). Eluent for chromatography: (5:95) ethyl acetate/dichloromethane. R_f = 0.47 [(5:95) ethyl acetate/dichloromethane]. Yield = 25 mg (23%). Pale yellow solid. Mp: 170–172 °C. ^{1}H NMR (500 MHz, $CDCl_3$) δ: 9.22 (s, 1H, NH), 8.50 (s, 1H, CH), 8.31 (d, *J* = 8.4 Hz, 1H, CH), 7.87 (d, *J* = 8.3 Hz, 2H, 2 × CH), 7.77 (d, *J* = 8.4 Hz, 1H, CH), 7.54–7.45 (m, 3H, 3 × CH), and 7.19 (s, 1H, CH) ppm. ^{13}C NMR (125 MHz, $CDCl_3$) δ: 146.7 (C), 142.0 (C), 136.3 (C), 135.9 (C), 129.5 (2 × CH), 129.5 (2 × CH), 129.0 (C), 128.3 (q, $J_{C\text{-}F}$ = 32 Hz, C), 127.9 (C), 127.4 (d, $J_{C\text{-}F}$ = 4 Hz, CH), 127.0 (CH), 125.2 (C), 124.4 (q, $J_{C\text{-}F}$ = 272 Hz, C), 124.0 (CH), 121.8 (d, $J_{C\text{-}F}$ = 3 Hz, CH), and 102.8 (CH) ppm. ^{19}F NMR (282 MHz, $CDCl_3$) δ: 62.0 (s, 3F, CF_3) ppm. MS (ESI) *m/z* = 347 (MH^+). HRMS calcd for $C_{18}H_{11}ClF_3N_2$ (MH^+): 347.0557; found, 347.0558.

*4.4.12. 4-(4-Chlorophenyl)-7-fluoro-3H-pyrrolo [2,3-c]quinoline (**54**)*

It was prepared according to the procedure described for compound **42** using: aniline **74** (70 mg, 0.40 mmol), 4-chlorobenzaldehyde (67 mg, 0.48 mmol). Eluent for chromatography: (5:95) ethyl acetate/dichloromethane. R_f = 0.32 [(5:95) ethyl acetate/dichloromethane]. Yield = 34 mg (29%). White solid. Mp: 146–147 °C. ^{1}H NMR (300 MHz, $CDCl_3$) δ: 9.37 (s, 1H, NH), 8.19 (dd, *J* = 8.9 and *J* = 6.1 Hz, 1H, CH), 7.84–7.75 (m, 3H, 3 × CH), 7.45 (t, *J* = 2.8 Hz, 1H, CH), 7.43–7.31 (m, 3H, 3 × CH), and 7.10 (t, *J* = 2.4 Hz, 1H, CH) ppm. ^{13}C NMR (125 MHz, $CDCl_3$) δ: 161.3 (d, $J_{C\text{-}F}$ = 244 Hz, C), 146.4 (C), 143.7 (d, $J_{C\text{-}F}$ = 12 Hz, C), 136.5 (C), 135.5 (C), 129.7 (C), 129.5 (2 × CH), 129.3 (2 × CH), 127.1 (CH), 126.9 (C), 124.6 (d, $J_{C\text{-}F}$ = 10 Hz, CH), 120.0 (C), 115.6 (d, $J_{C\text{-}F}$ = 25 Hz, CH), 113.5 (d, $J_{C\text{-}F}$ = 20 Hz, CH), and 102.1 (CH) ppm. ^{19}F NMR (282 MHz, $CDCl_3$) δ: 114.8 (s, 1F, CF) ppm. MS (ESI) *m/z* = 297 (MH^+). HRMS calcd for $C_{17}H_{11}ClFN_2$ (MH^+): 297.0589; found, 297.0590.

*4.4.13. 7-Chloro-4-(4-chlorophenyl)-3H-pyrrolo [2,3-c]quinoline (**55**)*

It was prepared according to the procedure described for compound **42** using: aniline **75** (50 mg, 0.26 mmol), 4-chlorobenzaldehyde (40 mg, 0.29 mmol). Eluent for chromatography: (30:70) ethyl acetate/hexane. R_f = 0.60 [(30:70) ethyl acetate/hexane]. Yield = 59 mg (72%). White solid. Mp: 177–179 °C. ^{1}H NMR (300 MHz, $CDCl_3$) δ: 9.26 (br s, 1H, NH), 8.16 (s, 1H, CH), 8.14 (d, *J* = 8.6 Hz, 1H, CH), 7.82 (d, *J* = 7.1 Hz, 2H, 2 × CH), 7.53 (dd, *J* = 8.6 and *J* = 1.8 Hz, 1H, CH), 7.47–7.42 (m, 3H, 3 × CH), and 7.11 (s, 1H, CH) ppm. ^{13}C NMR (125 MHz, $CDCl_3$) δ: 146.5 (C), 143.6 (C), 136.6 (C), 135.8 (C), 131.9 (C), 129.7 (2 × CH), 129.5 (2 x CH, C), 128.8 (CH), 127.4 (C), 127.1 (CH), 126.8 (CH), 124.4 (CH), 121.7 (C), and 102.5 (CH) ppm. MS (ESI) *m/z* = 313 (MH^+). HRMS calcd for $C_{17}H_{11}Cl_2N_2$ (MH^+): 313.0293; found, 313.0296.

*4.4.14. Methyl 4-(4-chlorophenyl)-3H-pyrrolo [2,3-c]quinoline-7-carboxylate (**56**)*

It was prepared according to the procedure described for compound **42** using: aniline **76** (100 mg, 0.46 mmol), 4-

chlorobenzaldehyde (78 mg, 0.56 mmol). Eluent for chromatography: (5:95) ethyl acetate/dichloromethane. R_f = 0.64 [(10:90) ethyl acetate/dichloromethane]. Yield = 94 mg (60%). White solid. Mp: 197–198 °C. ^{1}H NMR (500 MHz, DMSO-d_6) δ: 12.16 (br s, 1H, NH), 8.68 (d, J = 1.5 Hz, 1H, CH), 8.46 (d, J = 8.5 Hz, 1H, CH), 8.12–8.04 (m, 3H, 3 × CH), 7.74 (t, J = 2.8 Hz, 1H, CH), 7.69 (m, 2H, 2 × CH), 7.35 (dd, J = 2.7 and J = 1.6 Hz, 1H, CH), and 3.94 (s, 3H, CH_3) ppm. ^{13}C NMR (125 MHz, DMSO-d_6) δ: 166.4 (C), 146.3 (C), 141.1 (C), 136.4 (C), 134.2 (C), 131.2 (CH), 130.5 (2 × CH), 129.1 (CH), 128.7 (2 × CH), 128.6 (C), 127.2 (C), 126.8 (C), 126.1 (C), 124.9 (CH), 123.7 (CH), 102.0 (CH), and 52.1 (CH_3) ppm. MS (ESI) m/z = 337 (MH^+). HRMS calcd for $C_{19}H_{14}ClN_2O_2$ (MH^+): 337.0738; found, 337.0738.

4.4.15. 4-(4-Chlorophenyl)-7-methyl-3H-pyrrolo [2,3-c]quinoline (**57**)

It was prepared according to the procedure described for compound **42** using: aniline **77** (100 mg, 0.58 mmol), 4-chlorobenzaldehyde (98 mg, 0.70 mmol). Eluent for chromatography: gradient of ethyl acetate/hexane 1) (20:80), 2) (30:70). R_f = 0.35 [(30:70) ethyl acetate/hexane]. Yield = 133 mg (78%). White solid. Mp: 239–242 °C. ^{1}H NMR (500 MHz, $CDCl_3$) δ: 9.35 (br s, 1H, NH), 8.12 (d, J = 8.2 Hz, 1H, CH), 7.98 (s, 1H, CH), 7.79 (dd, J = 8.1 and J = 1.3 Hz, 2H, 2 × CH), 7.45–7.35 (m, 4H, 4 × CH), 7.10 (dd, J = 2.9 and J = 1.7 Hz, 1H, CH), and 2.56 (s, 3H, CH_3) ppm. ^{13}C NMR (125 MHz, $CDCl_3$) δ: 145.3 (C), 143.1 (C), 136.8 (C), 136.2 (C), 135.2 (C), 129.6 (C), 129.5 (2 × CH), 129.2 (2 × CH), 128.8 (CH), 128.1 (CH), 127.0 (C), 126.6 (CH), 122.7 (CH), 120.9 (C), 102.0 (CH), and 21.7 (CH_3) ppm. MS (ESI) m/z = 293 (MH^+). HRMS calcd for $C_{18}H_{14}ClN_2$ (MH^+): 293.0840; found, 293.0840.

4.5. Preparation of compounds **51** and **58**–**64**

4.5.1. 7-Methoxy-3-methyl-4-phenethyl-3H-pyrrolo [2,3-c] quinoline (**51**)

A solution of compound **50** (35 mg, 0.12 mmol) in dry THF (1.2 mL), at 0 °C and under argon, was treated with NaH (29 mg, 0.72 mmol, *ca* 60% in mineral oil) and stirred for 30 min. Iodomethane (45 μL, 0.72 mmol) was added and the resulting mixture was stirred at room temperature for 14 h. Water was added and THF was removed under reduced pressure. The resulting aqueous solution was acidified with HCl (10%) until pH 3, and then extracted with dichloromethane (3 ×). The combined organic extracts were dried (anh. Na_2SO_4), filtered and concentrated under reduced pressure. The reaction crude was purified by flash column chromatography, eluting with (10:90) ethyl acetate/hexane, to give compound **51** (27 mg, 73%), as a pale yellow solid. R_f = 0.52 [(10:90) ethyl acetate/dichloromethane]. Mp: 111–112 °C. ^{1}H NMR (300 MHz, $CDCl_3$) δ: 8.04 (d, J = 8.8 Hz, 1H, CH), 7.54 (d, J = 2.2 Hz, 1H, CH), 7.31 (d, J = 4.1 Hz, 4H, 4 × CH), 7.26 (s, 1H, CH), 7.22–7.18 (m, 1H, CH), 7.13 (d, J = 2.9 Hz, 1H, CH), 6.88 (t, J = 4.5 Hz, 1H, CH), 4.08 (s, 3H, CH_3), 3.98 (s, 3H, CH_3), 3.68–3.62 (m, 2H, CH_2), and 3.31–3.25 (m, 2H, CH_2) ppm. ^{13}C NMR (75 MHz, $CDCl_3$) δ: 158.4 (C), 148.8 (C), 143.5 (C), 141.7 (C), 132.7 (CH), 131.2 (C), 128.7 (2 × CH), 128.6 (2 × CH), 128.0 (C), 126.3 (CH), 123.7 (CH), 117.5 (C), 117.5 (CH), 108.0 (CH), 99.5 (CH), 55.6 (CH_3), 37.9 (CH_2), 37.5 (CH_2), and 36.2 (CH_3) ppm. MS (ESI) m/z = 317 (MH^+). HRMS calcd for $C_{21}H_{21}N_2O$ (MH^+): 317.1648; found, 317.1650.

4.5.2. 4-(4-Chlorophenyl)-3-methyl-3H-pyrrolo [2,3-c]quinoline (**58**)

It was prepared according to the procedure described for compound **51** using: compound **19** [29] (42 mg, 0.15 mmol), iodomethane (56 μL, 0.90 mmol). Eluent for chromatography: 20:80) ethyl acetate/hexane. Yield = 22 mg (50%). White solid. R_f = 0.51 [(20:80) ethyl acetate/hexane]. Mp: 215–217 °C. ^{1}H NMR (300 MHz, $CDCl_3$) δ: 8.24–8.18 (m, 2H, 2 × CH), 7.64–7.55 (m, 4H, 4 × CH), 7.53–7.49 (m, 2H, 2 × CH), 7.21 (d, J = 2.9 Hz, 1H, CH), 7.07 (d, J = 2.9 Hz, 1H, CH), and 3.47 (s, 3H, CH_3) ppm. ^{13}C NMR (75 MHz, $CDCl_3$) δ: 146.8 (C), 142.0 (C), 138.5 (C), 135.0 (C), 132.9 (CH), 130.9 (C), 130.9 (2 × CH), 129.7 (CH), 128.6 (2 × CH), 128.2 (C), 126.5 (CH), 126.2 (CH), 123.3 (C), 122.7 (CH), 100.5 (CH), and 37.4 (CH_3) ppm. MS (ESI) m/z = 293 (MH^+). HRMS calcd for $C_{18}H_{14}ClN_2$ (MH^+): 293.0840; found, 293.0838.

4.5.3. 4-(4-Chlorophenyl)-7-fluoro-3-methyl-3H-pyrrolo [2,3-c] quinoline (**59**)

It was prepared according to the procedure described for compound **51** using: compound **54** (35 mg, 0.12 mmol), iodomethane (44 μL, 0.71 mmol). Eluent for chromatography: (20:80) ethyl acetate/hexane. R_f = 0.40 [(20:80) ethyl acetate/hexane]. Yield = 21 mg (57%). Pale yellow solid. Mp: 223–225 °C. ^{1}H NMR (300 MHz, $CDCl_3$) δ: 8.19 (dd, J = 8.8 and J = 6.1 Hz, 1H, CH), 7.81 (dd, J = 10.6 and J = 2.3 Hz, 1H, CH), 7.60–7.48 (m, 4H, 4 × CH), 7.36 (td, J = 8.5 and J = 2.2 Hz, 1H, CH), 7.26 (s, 1H, CH), 7.02 (d, J = 2.8 Hz, 1H, CH), and 3.47 (s, 3H, CH_3) ppm. ^{13}C NMR (75 MHz, $CDCl_3$) δ: 161.4 (d, $J_{C\text{-}F}$ = 245 Hz, CF), 147.8 (C), 142.8 (C), 135.2 (C), 133.5 (CH), 131.1 (C), 130.8 (2 × CH), 128.9 (C), 128.7 (2 × CH), 127.9 (C), 124.4 (d, $J_{C\text{-}F}$ = 9 Hz, CH), 120.1 (C), 115.8 (d, $J_{C\text{-}F}$ = 24 Hz, CH), 113.6 (d, $J_{C\text{-}F}$ = 21 Hz, CH), 100.3 (CH), and 37.5 (CH_3) ppm. ^{19}F NMR (282 MHz, $CDCl_3$) δ: 115.0 (q, J = 7.6 Hz, 1F, CF) ppm. MS (ESI) m/z = 311 (MH^+). HRMS calcd for $C_{18}H_{13}ClFN_2$ (MH^+): 311.0744; found, 311.0745.

4.5.4. 4-(4-Chlorophenyl)-3-(cyclopropylmethyl)-7-fluoro-3H-pyrrolo [2,3-c]quinoline (**60**)

It was prepared according to the procedure described for compound **51** using: compound **54** (35 mg, 0.12 mmol), (iodomethyl) cyclopropane (84 μL, 0.71 mmol). Eluent for chromatography: gradient of ethyl acetate/hexane: 1) (5:95), 1) (15:85). R_f = 0.51 [(10:90) ethyl acetate/hexane]. Yield = 31 mg (75%). White solid. Mp: 114–116 °C. ^{1}H NMR (500 MHz, $CDCl_3$) δ: 8.19 (dd, J = 8.9 and J = 6.0 Hz, 1H, CH), 7.82 (dd, J = 10.5 and J = 2.5 Hz, 1H, CH), 7.59–7.55 (m, 2H, 2 × CH), 7.53–7.49 (m, 2H, 2 × CH), 7.49 (d, J = 3.0 Hz, 1H, CH), 7.36 (td, J = 8.6 and J = 2.6 Hz, 1H, CH), 7.07 (d, J = 3.0 Hz, 1H, CH), 3.66 (d, J = 6.9 Hz, 2H, CH_2), 0.96–0.81 (m, 1H, CH), 0.52–0.41 (m, 2H, CH_2), and 0.15–0.06 (m, 2H, CH_2) ppm. ^{13}C NMR (125 MHz, $CDCl_3$) δ: 161.4 (d, $J_{C\text{-}F}$ = 244 Hz, CF), 147.7 (C), 142.8 (d, $J_{C\text{-}F}$ = 12 Hz, C), 138.5 (C), 135.1 (C), 131.8 (CH), 131.4 (C), 130.6 (2 × CH), 128.8 (2 × CH), 127.4 (C), 124.4 (d, $J_{C\text{-}F}$ = 9 Hz, CH), 120.0 (C), 115.7 (d, $J_{C\text{-}F}$ = 25 Hz, CH), 113.5 (d, $J_{C\text{-}F}$ = 20 Hz, CH), 100.5 (CH), 53.4 (CH_2), 11.8 (CH), and 4.2 (2 × CH_2) ppm. ^{19}F NMR (282 MHz, $CDCl_3$) δ: 115.1 (q, J = 7.9 Hz, 1F, CF) ppm. MS (ESI) m/z = 351 (MH^+). HRMS calcd for $C_{21}H_{17}ClFN_2$ (MH^+): 351.1058; found, 351.1062.

4.5.5. 4-(4-Chlorophenyl)-3,7-dimethyl-3H-pyrrolo [2,3-c] quinoline (**61**)

It was prepared according to the procedure described for compound **51** using: compound **57** (35 mg, 0.12 mmol), iodomethane (45 μL, 0.72 mmol). Eluent for chromatography: (20:80) ethyl acetate/hexane. R_f = 0.37 [(20:80) ethyl acetate/hexane]. Yield = 15 mg (39%). Pale yellow solid. Mp: 112–113 °C. ^{1}H NMR (500 MHz, $CDCl_3$) δ: 8.11 (d, J = 8.2 Hz, 1H, CH), 8.02 (s, 1H, CH), 7.57 (m, 2H, 2 × CH), 7.50 (m, 2H, 2 × CH), 7.43 (d, J = 8.2 Hz, 1H, CH), 7.21 (d, J = 2.6 Hz, 1H, CH), 7.03 (d, J = 2.7 Hz, 1H, CH), 3.47 (s, 3H, CH_3), and 2.57 (s, 3H, CH_3) ppm. ^{13}C NMR (125 MHz, $CDCl_3$) δ: 146.6 (C), 142.0 (C), 138.5 (C), 136.4 (C), 135.0 (C), 133.1 (CH), 131.0 (C), 130.9 (2 × CH), 128.8 (CH), 128.6 (2 × CH), 128.2 (CH), 128.0 (C), 122.5 (CH), 121.0 (C), 100.2 (CH), 37.5 (CH_3), and 21.8 (CH_3) ppm. MS (ESI) m/z = 307 (MH^+). HRMS calcd for $C_{19}H_{16}ClN_2$ (MH^+): 307.0996; found, 307.0993.

4.5.6. 1-Chloro-4-(4-chlorophenyl)-3H-pyrrolo [2,3-c]quinoline (**62**)

A solution of compound **19** [29] (41 mg, 0.15 mmol) in DMF (150 μL) at room temperature was treated with *N*-chlorosuccinimide (20 mg, 0.15 mmol) and the resulting mixture was heated at reflux for 3 h. After cooling to room temperature, the DMF was removed under reduced pressure and the resulting residue was dissolved with ethyl acetate, and then washed with brine (3 ×). The organic extract was dried (anh. Na_2SO_4), filtered and concentrated under reduced pressure. The reaction crude was purified by flash column chromatography on silica gel, eluting with (20:80) ethyl acetate/hexane, to give compound **62** (30 mg, 64%), as a pale yellow solid. $R_f = 0.50$ [(20:80) ethyl acetate/hexane]. Mp: 146–148 °C. ^{1}H NMR (300 MHz, $(CD_3)_2CO$) δ: 8.94 (m, 1H, CH), 8.17 (m, 1H, CH), 8.07 (m, 2H, 2 × CH), 7.74 (s, 1H, CH), and 7.72–7.59 (m, 4H, 4 × CH) ppm. ^{13}C NMR (75 MHz, $(CD_3)_2CO$) δ: 146.5 (C), 144.2 (C), 137.7 (C), 135.8 (C), 131.3 (2 × CH), 130.9 (CH), 129.8 (2 × CH), 127.3 (CH), 127.0 (CH), 126.0 (CH), 125.8 (C), 124.5 (C), 123.6 (C), 123.1 (CH), and 107.8 (C) ppm. MS (ESI) m/z = 313 (MH^+). HRMS calcd for $C_{17}H_{11}Cl_2N_2$ (MH^+): 313.0294; found, 313.0292.

4.5.7. 1-Bromo-4-(4-chlorophenyl)-3H-pyrrolo [2,3-c]quinoline (**63**)

A solution of compound **19** [29] (100 mg, 0.36 mmol) in (80:20) THF/H_2O (12 mL) at room temperature was treated with *N*-bromosuccinimide (64 mg, 0.36 mmol) and the resulting mixture was stirred vigorously for 15 min. The reaction mixture was diluted with water (6 mL) and extracted with ethyl acetate (3 ×). The combined organic extracts were dried (anh. Na_2SO_4), filtered and concentrated under reduced pressure. The reaction crude was purified by flash column chromatography on silica gel, eluting with (20:80) ethyl acetate/hexane, to give compound **63** (102 mg, 79%), as a pale yellow solid. R_f = 0.52 [(20:80) ethyl acetate/hexane]. Mp: 174–176 °C. ^{1}H NMR (300 MHz, $(CD_3)_2CO$) δ: 11.42 (br s, 1H, NH), 9.12 (m, 1H, CH), 8.18 (m, 1H, CH), 8.07 (m, 2H, 2 × CH), 7.78 (s, 1H, CH), and 7.73–7.59 (m, 4H, 4 × CH) ppm. ^{13}C NMR (75 MHz, $(CD_3)_2CO$) δ: 162.3 (C), 144.1 (C), 137.6 (C), 135.7 (C), 131.3 (2 × CH), 130.9 (CH), 129.8 (2 × CH), 128.7 (CH), 128.5 (C), 127.3 (CH), 126.8 (CH), 125.4 (C), 123.7 (C), 122.5 (CH), and 91.2 (C) ppm. MS (ESI) m/z = 357 and 359 (MH^+). HRMS calcd for $C_{17}H_{11}^{79}BrClN_2$ (MH^+): 356.9789; found, 356.9787.

4.5.8. 4-(4-Chlorophenyl)-1-(3-fluorophenyl)-3H-pyrrolo [2,3-c] quinoline (**64**)

A suspension of bromide **63** (30 mg, 84 μmol), $Pd(PPh_3)_4$ (10 mg, 8 μmol), (3-fluorophenyl)boronic acid (18 mg, 0.13 mmol), and K_2CO_3 (27 mg, 0.13 mmol) in a mixture of (80:20) dioxane/water (0.5 mL) was heated at 90 °C for 14 h. After cooling to room temperature, the reaction mixture was diluted with water and ethyl acetate. The aqueous layer was separated, and the organic layer was washed with brine, dried (anh. Na_2SO_4), filtered and concentrated under reduced pressure. The reaction crude was purified by flash column chromatography on silica gel, eluting with a gradient of ethyl acetate/hexane: 1) (15:85); 2) (20:80), to give compound **64** (13 mg, 42%), as a white solid. R_f = 0.47 [(20:80) ethyl acetate/hexane]. Mp: 98–100 °C. ^{1}H NMR (500 MHz, $CDCl_3$) δ: 9.16 (br s, 1H, NH), 8.22 (d, J = 8.3 Hz, 1H, CH), 8.10 (d, J = 8.2 Hz, 1H, CH), 7.89 (d, J = 8.2 Hz, 2H, 2 × CH), 7.58 (t, J = 7.6 Hz, 1H, CH), 7.53 (d, J = 8.2 Hz, 2H, 2 × CH), 7.51–7.45 (m, 1H, CH), 7.44–7.28 (m, 4H, 4 × CH), and 7.16 (td, J = 8.5 and J = 2.6 Hz, 1H, CH) ppm. ^{13}C NMR (125 MHz, $CDCl_3$) δ: 163.0 (d, $J_{C\text{-}F}$ = 247 Hz, C), 145.9 (C), 143.7 (C), 137.9 (d, $J_{C\text{-}F}$ = 7 Hz, C), 136.7 (C), 135.7 (C), 130.2 (CH), 130.0 (CH), 129.8 (2 × CH), 129.6 (2 × CH), 127.7 (C), 126.6 (CH), 126.0 (CH), 125.9 (CH), 125.8 (C), 125.5 (CH), 123.5 (C), 123.1 (CH), 120.5 (C), 117.0 (d, $J_{C\text{-}F}$ = 21 Hz, CH), and 114.5 (d, $J_{C\text{-}F}$ = 21 Hz, CH) ppm. ^{19}F NMR (282 MHz, $CDCl_3$) δ: 109.5 (q, J = 7.1 Hz, 1F, CF) ppm. MS (ESI) m/z = 373 (MH^+). HRMS calcd for $C_{23}H_{15}ClFN_2$ (MH^+): 373.0902; found, 373.0901.

4.6. In vitro studies

The *in vitro* antibacterial activity of natural marinoquinoline A (**1**), B (**2**), C (**3**) and E (**5**) as well as compounds **8**–**40** and **42**–**64** was studied by determining their minimum inhibitory concentrations (MIC) against *M. tuberculosis* H37Rv. Mycobacterial strains were cultured in Middlebook 7H9 broth, supplemented with 0.5% glycerol and 10% ADC (albumin, dextrose, catalase), and incubated at 37 °C. For susceptibility tests, cultures were diluted to 10^5 cells/mL and assayed against a series of 2-fold concentrations of compounds, from 160 to 1.25 μg/mL; growth was recorded by using the Alamar Blue Assay after eight days [34]. MIC values were defined as the lowest concentration at which bacterial growth was no longer evident. All assays were done in duplicate. MIC value of the reference drug moxifloxacin was also determined for comparison.

4.7. Enzymatic assays with glutamate 5-kinase

G5K from *E. coli* was purified as described previously [54]. For assays, aliquots of the enzyme stock solutions of 0.15 mg/mL concentration were prepared by dilution from the stock in Tris.HCl (50 mM, pH 7.0), imidazole (100 mM, pH 7.0), ammonium sulfate (12 mM), dithiothreitol (1 mM) and bovine serum albumin (0.9 mg/mL) and stored on ice. Enzyme activity was measured at 37 °C by monitoring the oxidation of NADH to NAD in a coupled assay format wherein ADP produced was detected using pyruvate kinase (PK) and lactate dehydrogenase (LDH) enzymes [55]. To this end, the decrease in absorbance at 340 nm in the UV spectrum due to NADH (ε/M^{-1} cm^{-1} 6220) was monitored. Standard assay conditions for G5K were Tris.HCl (50 mM, pH 7.0), dithiothreitol (1 mM), $MgCl_2$ (70 mM), ATP (10 mM), sodium L-glutamate (10 mM), phosphoenolpyruvate monopotassium salt (5 mM), NADH (0.25 mM), bovine serum albumin (1 mg/mL), PK (from rabbit muscle, 80 μg/mL), and LDH (from rabbit muscle, 30 μg/mL). Each assay was initiated by addition of aliquots of G5K. Solutions of ATP and NADH were calibrated by measuring the absorbance at 259 nm and 340 nm in the UV spectrum, respectively.

For inhibition assays, aliquots of stock solutions of compounds **50** and **54** in DMSO (20 mM) were employed. At the maximum concentrations used, DMSO, L-proline, **50** or **54** did not inhibit the coupled PK/LDH enzymatic system as no significant changes in activity were observed when adding extra quantities of the coupled enzymes. At the maximal concentrations used (0.6%), DMSO did not affect G5K activity. The initial rates at fixed enzyme and substrate concentrations were measured in the absence and in the presence of various compounds concentrations. Compounds **50** and **54** and the natural inhibitor L-Pro were employed.

The program GraphPad Prism (GraphPad Software, San Diego, CA) was used for data fitting. The inhibition data was adjusted to sigmoidal inhibition (equation (1)):

$$\upsilon_{[Inh]} = \upsilon_{[Inh]=\infty} + (\upsilon_{[Inh]=0} - \upsilon_{[Inh]=\infty}) \times (1 - ([Inh]^N/(I_{0.5}^N + [Inh]^N))) \quad (1)$$

where $\upsilon_{[Inh]}$ is the velocity at a given concentration of the inhibitor, $\upsilon_{[Inh]=0}$ and $\upsilon_{[Inh]=\infty}$ are the activities in the absence and at infinite concentration of the inhibitor, N is the Hill coefficient, [Inh] is the inhibitor concentration, $I_{0.5}$ is the concentration of the inhibitor at which $\upsilon_{[Inh]} = \upsilon_{[Inh]=\infty} + (\upsilon_{[Inh]=0} - \upsilon_{[Inh]=\infty})/2$.

For convenience, activities are expressed as percentage of the activity in the absence of inhibitors. Assay results are given as the means ± S.E. of at least three determinations.

For 10 mM concentration of L-Glu and ATP, $I_{0.5}$ values for L-proline, compound **50** and compound **54** were 2.5 ± 0.3 μM, 22.1 ± 0.7 μM and 33 ± 12 μM, respectively. For all three inhibitors the sigmoidicity of the concentration-activity curves was modest, showing N values of 1.39 ± 0.24, 1.40 ± 0.05 and 1.4 ± 0.7, respectively.

4.8. Cytotoxicity assays

These studies were performed on HepG2 cell line (human hepatocellular carcinoma cells), which were grown on culture medium EMEM (Eagle's Minimum Essential Medium) supplemented with 10% FBS (Fetal Bovine Serum) in an atmosphere of 95% air and 5% CO_2 at 37 °C. The inhibition of cell growth induced by compounds **50** and **54** was evaluated using the MTT [3-(4,5-dimethylthiazol-2-yl)-2,5-diphenyltetrazolium bromide] assay. The cells were seeded in a sterile 96-well plate at a density of 10.000 cells/well and incubated for 24 h in growth medium. A solution of compounds **50** and **54** in DMSO, at 5 μM, 10 μM and 20 μM concentration, was added to the cells maintaining the same proportion of solvent in each well. After 48 h of incubation in an atmosphere of 95% air and 5% CO_2 at 37 °C, 10 μL of a solution of MTT (5 mg/mL) in PBS (136 mM NaCl, 1.47 mM KH_2PO_4, 8 mM NaH_2PO_4 and 2.68 mM KCl) was added to each well and the cell plate was incubated for another 4 h. Next, 100 μL of 10% SDS prepared in 10 mM HCl was added and cell plate was incubated for 12–14 h under the same experimental conditions. Finally, absorbance of the cell plate was measured at a wavelength of 595 nm in a Tecan M1000 infinite Pro microplate reader. All experiments were performed by triplicate. The absorbance measurement range was assessed between 1 value (average of triplicate points) containing 10.000 cells in EMEM and in the absence of growth factors, which determine the stable cell concentration, and another value (average of triplicate points) containing the usual growth medium, which allows to stablish the maximum cell growth at 48 h. Controls with DMSO at the same proportion in which the compounds were dissolved were also performed. These controls showed an inhibition of cell growth of 6–8% relative to the control in which the cells were grown in the usual growth medium.

The percentage of inhibition was calculated using the equation (2)

$$\% \text{ inhibition} = 100 - (AO \times 100/AT) \quad (2)$$

where AO is the absorbance observed in the wells in the presence of compound **50** or **54** and AT is the absorbance obtained in the wells with DMSO controls. As a control, the inhibitory potency of cisplatin was measured by calculation the concentration-% inhibition curve, which was adjusted to the equation (3):

$$y = E_{max} / 1 + (IC_{50} / x)^n \quad (3)$$

were y is the observed effect at a concentration x, E_{max} corresponds to the maximum effect, IC_{50} is the concentration at which a 50% growth inhibition is obtained, and n is the slope of the curve. The program GraphPad Prism was used for data fitting. For the evaluation of cisplatin, two parameters were used: the inhibitory potency ($1/IC_{50}$) and efficacy (expressed as maximum % inhibition reached by the compound). Under these experimental conditions, the values obtained for cisplatin were E_{max} (%) = 63 ± 2 and IC_{50} (μM) = 6.3 ± 0.1.

4.9. Computational studies

4.9.1. MD simulations studies of G5K enzymes in the unbound form

For the *E. coli* enzyme, the available three-dimensional structure of *Ec*-G5K in complex with glutamate (PDB 2J5T, 2.9 Å; chain E) was employed [45]. Computation of the protonation state of titratable groups at pH 7.0 was carried out using the H^{++} Web server [56]. As a result of this analysis: His27, His39, His43, His59, His97, His256, His325, His341, His342, and His360 were protonated in ε position. Cysteine residues Cys35, Cys225 and Cys316 were considered in the free form. To model the three-dimensional structure of *Mt*-G5K, the web-based homology modelling Phyre2 server was used [47]. In this case, the histidine residues His114, His122, His136, His166, His215, and His361, were protonated in ε position, and the cysteine residues Cys185 and Cys313 were considered in the free form.

Next, the minimization of the enzyme models and MD simulation of the resulting minimized structures were carried out following our previously described protocol [57]. 100 ns simulations were performed. The cpptraj module in AMBER 17 was used to analyze the trajectories and to calculate the rmsd of the protein during the simulation (Fig. S8) [58]. The molecular graphics program PyMOL [59] was employed for visualization and depicting enzyme structures.

4.9.2. Building of the Ligand@G5K binary complexes

(1) *Ligand preparation.* The ligand geometries were minimized using a restricted Hartree-Fock (RHF) method and a 6-31G(d) basis set, as implemented in the ab initio program Gaussian 09 [60]. Partial charges were derived by quantum mechanical calculations using Gaussian 09, as implemented in the R.E.D. Server (version 3.0) [61–63], according to the RESP [64] model. The missing bonded and nonbonded parameters were assigned, by analogy or through interpolation, from those already present in the AMBER database (GAFF) [65,66].

(2) *Docking studies:* The binding mode of compounds **50** and **54** were first explored by docking using program GOLD 2020.2.0 [48] and the coordinates of both G5K enzymes in the unbound form. The snapshot after 90 ns of simulation was selected as no relevant changes in the AAK domain and the linker region was observed. The ligand geometries previously minimized were used as MOL2 files. Each ligand was docked in 25 independent genetic algorithm (GA) runs, and for each of these, a maximum number of 100,000 GA operations were performed on a single population of 50 individuals. Operator weights for crossover, mutation, and migration in the entry box were used as default parameters (95, 95, and 10, respectively) as well as the hydrogen bonding (4.0 Å) and van der Waals (2.5 Å) parameters. The position of Ala226 was used to define the active site, and the radius was set to 6 Å. The GOLD scoring function was used.

4.9.3. MD simulations studies of Ligand@G5K binary complexes

(1) *Minimization of the ligand@G5K binary complexes*: Ligand coordinates obtained by docking were employed as starting point for MD simulations of the corresponding binary complexes. The complexes immersed in a truncated octahedron of TIP3P water molecules and sodium ions were minimized in four stages: (1) initial minimization of the ligands (1000 steps, first half using steepest descent and the rest using conjugate gradient); steps (2), (3) and (4) were performed as steps (a), (b) and (c) in the minimization of the unbound form. A positional restraint force of 50 kcal mol^{-1} $Å^{-2}$ was

applied to those unminimized atoms during the first three stages (1–3).

(2) *Simulations of the ligand(s)@G5K enzyme complexes*: MD simulations of the binary complexes [**50**@G5K, **54**@G5K], Michaelis complexes [Glu + ATP + Mg^{2+}@G5K] and quaternary complexes [**50** + Glu + ATP + Mg^{2+}@G5K, **54** + Glu + ATP + Mg^{2+}@G5K] were performed as indicated for the unbound protein form during 100 ns.

4.9.4. Vibrational modes calculations

The vibrational modes for: (i) G5K in the unbound form; (ii) Michaelis complexes; (iii) ligand@ G5K binary enzyme complexes; were calculated from the corresponding MD trajectories by principal component analysis using the cpptraj module [67].

4.9.5. Binding free energies calculations

The binding free energy for ATP was calculated by the MM/PBSA approach implemented in Amber Tools 1.5 [68]. ante-MMPBSA.py module was used to create topology files for the complex, enzyme and ligands and binding free energies were calculated with the MMPBSA.py module. A single trajectory approach was used to calculate binding free energies considering only the last 80 ns of the 100 ns MD trajectories. The Poisson-Boltzmann (PB) and Generalized Born (GB) implicit solvation models were employed. Both models provided similar results.

Declaration of competing interest

The authors declare that they have no known competing financial interests or personal relationships that could have appeared to influence the work reported in this paper.

Acknowledgments

Financial support from the Spanish Ministry of Science and Innovation (PID2019-105512RB-I00, CG-B), Axencia Galega de Innovación (2020-PG067, CG-B), the Xunta de Galicia [ED431C 2021/29 and the Centro singular de investigación de Galicia accreditation 2019–2022 (ED431G 2019/03), CG-B], and the European Regional Development Fund (ERDF) is gratefully acknowledged. MP and CRDC thank the Fundação de Amparo à Pesquisa do estado de São Paulo (FAPESP) for a postdoctoral fellowship (2016/23055-3), and research grants (2014/25770-6, 2013/07600-3). CRDC also thanks the Brazilian National Research Council (CNPq) (grants 406642/2018-0, 306773/2018-0). AR thanks the Spanish Ministry of Economy, Industry and Competitiveness for her FPI fellowship (BES-2017-080946). VR thanks the Fundación Ramón Areces (Ciencias de la Vida, XX National call). All authors are grateful to the Centro de Supercomputación de Galicia (CESGA) for use of the Finis Terrae computer.

Appendix A. Supplementary data

Supplementary data to this article can be found online at https://doi.org/10.1016/j.ejmech.2022.114206.

Abbreviations

G5K	glutamate-5-kinase
Ec-G5K	glutamate-5-kinase from *Escherichia coli*
Mt-G5K	glutamate-5-kinase from *Mycobacterium tuberculosis*
MD	Molecular Dynamics
MDR	multidrug-resistant
TB	tuberculosis
XDR	extensively drug-resistant

References

[1] J. Furin, H. Cox, M. Pai, Tuberculosis, Lancet 393 (2019) 1642–1656, https://doi.org/10.1016/S0140-6736(19)30308-3.
[2] S. Tiberi, N. du Plessis, G. Walzl, M.J. Vjecha, M. Rao, F. Ntoumi, S. Mfinanga, N. Kapata, P. Mwaba, T.D. McHugh, G. Ippolito, G.B. Migliori, M.J. Maeurer, A. Zumla, Tuberculosis: progress and advances in development of new drugs, treatment regimens, and host-directed therapies, Lancet Infect. Dis. 18 (2018) e183–e198, https://doi.org/10.1016/S1473-3099(18)30110-5.
[3] T.J. Scriba, V. Mizrahi, Renewing the fight against TB with an old vaccine, Cell 180 (2020) 829–831, https://doi.org/10.1016/j.cell.2020.02.024.
[4] M. Pai, M. Behr, D. Dowdy, K. Dheda, M. Divangahi, C.C. Boehme, A. Ginsberg, S. Swaminathan, M. Spiegelmam, H. Getahun, D. Menzies, M. Raviglione, Tuberculosis, Nat. Rev. Dis. Primers 2 (2016) 16076, https://doi.org/10.1038/nrdp.2016.76.
[5] R.M.G.J. Houben, P.J. Dodd, The global burden of latent tuberculosis infection: a re-estimation using mathematical modelling, PLoS Med. 13 (2016), e1002152, https://doi.org/10.1371/journal.pmed.1002152.
[6] R. Waters, M. Ndengane, M.-R. Abrahams, C.R. Diedrich, R.J. Wilkinson, A.K. Coussens, The Mtb-HIV syndemic interaction: why treating M. tuberculosis infection may be crucial for HIV-1 eradication, Future Virol. 15 (2020) 101–126, https://doi.org/10.2217/fvl-2019-0069.
[7] L.C.K. Bell, M. Noursadeghi, Pathogenesis of HIV-1 and Mycobacterium tuberculosis co-infection, Nat. Rev. Microbiol. 16 (2018) 80–90, https://doi.org/10.1038/nrmicro.2017.128.
[8] WHO, Tuberculosis. https://www.who.int/news-room/fact-sheets/detail/tuberculosis, 2021. (Accessed 23 December 2021).
[9] WHO, Global tuberculosis report 2020. https://www.who.int/publications/i/item/9789240013131, 2021. (Accessed 23 December 2021).
[10] WHO, Global Priority list of antibiotic-resistant bacteria to guide research, discovery, and development of new antibiotics, February 27, 2017, http://www.who.int/medicines/publications/WHO-PPL-Short_Summary_25Feb-ET_NM_WHO.pdf?ua=1, 2021. (Accessed 23 December 2021).
[11] E.D. Brown, G.D. Wright, Antibacterial drug discovery in the resistance era, Nature 529 (2016) 336–343, https://doi.org/10.1038/nature17042.
[12] T.J. de Wet, D.F. Warner, V. Mizrahi, Harnessing biological insight to accelerate tuberculosis drug discovery, Acc. Chem. Res. 52 (2019) 2340–2348, https://doi.org/10.1021/acs.accounts.9b00275.
[13] M.G. Moloney, Natural products as a source for novel antibiotics, Trends Pharmacol. Sci. 37 (2016) 689–701, https://doi.org/10.1016/j.tips.2016.05.001.
[14] A. Harvey, R. Edrada-Ebel, R. Quinn, The re-emergence of natural products for drug discovery in the genomics era, Nat. Rev. Drug Discov. 14 (2015) 111–129, https://doi.org/10.1038/nrd4510.
[15] T. Molinski, D. Dalisay, S. Lievens, J.P. Saludes, Drug development from marine natural products, Nat. Rev. Drug Discov. 8 (2009) 69–85, https://doi.org/10.1038/nrd2487.
[16] E. Brown, G. Wright, Antibacterial drug discovery in the resistance era, Nature 529 (2016) 336–343, https://doi.org/10.1038/nature17042.
[17] T. Rodrigues, D. Reker, P. Schneider, G. Schneider, Counting on natural products for drug design, Nat. Chem. 8 (2016) 531–541, https://doi.org/10.1038/nchem.2479.
[18] J.J. Hug, D. Krug, R. Müller, Bacteria as genetically programmable producers of bioactive natural products, Nat. Rev. Chem. 4 (2020) 172–193, https://doi.org/10.1038/s41570-020-0176-1.
[19] G. Karageorgis, D.J. Foley, L. Laraia, H. Waldmann, Principle and design of pseudo-natural products, Nat. Chem. 12 (2020) 227–235, https://doi.org/10.1038/s41557-019-0411-x.
[20] D.J. Newman, G.M. Cragg, Natural products as sources of new drugs over the nearly four decades from 01/1981 to 09/2019, J. Nat. Prod. 83 (2020) 770–803, https://doi.org/10.1021/acs.jnatprod.9b01285.
[21] M.A. Riva, From milk to rifampicin and back again: history of failures and successes in the treatment for tuberculosis, J. Antibiot 67 (2014) 661–665, https://doi.org/10.1038/ja.2014.108.
[22] G.D. Wright, Unlocking the potential of natural products in drug discovery, Microb, Biotechnol. 12 (2019) 55–57, https://doi.org/10.1111/1751-7915.13351.
[23] G.D. Wright, Opportunities for natural products in 21st century antibiotic discovery, Nat. Prod. Rep. 34 (2017) 694–701, https://doi.org/10.1039/c7np00019g.
[24] P.W. Okanya, K.I. Mohr, K. Gerth, R. Jansen, R. Müller, Marinoquinolines A–F, pyrroloquinolines from ohtaekwangia kribbensis (bacteroidetes), J. Nat. Prod. 74 (2011) 603–608, https://doi.org/10.1021/np100625a.
[25] Y. Sangnoi, O. Sakulkeo, S. Yuenyongsawad, A. Kanjana-opas, K. Ingkaninan, A. Plubrukarn, K. Suwanborirux, Acetylcholinesterase-inhibiting activity of pyrrole derivatives from a novel marine gliding bacterium Rapidithrix thailandica, Mar. Drugs 6 (2008) 578–586, https://doi.org/10.3390/md20080029.
[26] E.J. Choi, S.J. Nam, L. Paul, D. Beatty, C.A. Kauffman, P.R. Jensen, W. Fenical, Previously uncultured marine bacteria linked to novel alkaloid production, Chem. Biol. 22 (2015) 1270–1279, https://doi.org/10.1016/j.chembiol.2015.07.014.
[27] B. Bolte, C.S. Bryan, P.P. Sharp, S. Sayyahi, C. Rihouey, A. Kendrick, P. Lan, M.G. Banwell, C.J. Jackson, N.J. Fraser, A.C. Willis, J.S. Ward, C.J. Jackson, Total syntheses of the 3H-pyrrolo[2,3-c]quinolone-containing alkaloids

Marinoquinolines A-F, K, and Aplidiopsamine A using a palladium-catalyzed ullmann cross-coupling/reductive cyclization pathway, J. Org. Chem. 85 (2020) 650–663, https://doi.org/10.1021/acs.joc.9b02725.
[28] A.R. Carroll, S. Duffy, V.M. Avery, Aplidiopsamine A, an antiplasmodial alkaloid from the temperate Australian ascidian, Aplidiopsis confluata, J. Org. Chem. 75 (2010) 8291–8294, https://doi.org/10.1021/jo101695v.
[29] A.C.C. Aguiar, M. Panciera, E.F.S. dos Santos, M.K. Singh, M.L. Garcia, G.E. de Souza, M. Nakabashi, J.L. Costa, C.R.S. Garcia, G. Oliva, C.R.D. Correia, R.V.C. Guido, Discovery of marinoquinolines as potent and fast-acting Plasmodium falciparum inhibitors with in vivo activity, J. Med. Chem. 61 (2018) 5547–5568, https://doi.org/10.1021/acs.jmedchem.8b00143.
[30] S.S. Gholap, Pyrrole: an emerging scaffold for construction of valuable therapeutic agents, Eur. J. Med. Chem. 110 (2016) 13–31, https://doi.org/10.1016/j.ejmech.2015.12.017.
[31] A. Koul, N. Dendouga, K. Vergauwen, B. Molenberghs, L. Vranckx, R. Willebrords, Z. Ristic, H. Lill, I. Dorange, J. Guillemont, D. Bald, K. Andries, Diarylquinolines target subunit c of mycobacterial ATP synthase, Nat. Chem. Biol. 3 (2007) 323–324, https://doi.org/10.1038/nchembio884.
[32] E. Pitta, M.K. Rogacki, O. Balabon, S. Huss, F. Cunningham, E.M. Lopez-Roman, J. Joossens, K. Augustyns, L. Ballell, R.H. Bates, P. van der Veken, Searching for new leads for tuberculosis: design, synthesis, and biological evaluation of novel 2-quinolin-4-yloxyacetamides, J. Med. Chem. 59 (2016) 6709–6728, https://doi.org/10.1021/acs.jmedchem.6b00245.
[33] G.G. Makafe, M. Hussain, G. Surineni, Y. Tan, N.K. Wong, M. Julius, L. Liu, C. Gift, H. Jiang, Y. Tang, J. Liu, S. Tan, Z. Yu, Z. Liu, Z. Lu, C. Fang, Y. Zhou, J. Zhang, Q. Zhu, J. Liu, T. Zhang, Quinoline derivatives kill Mycobacterium tuberculosis by activating glutamate kinase, Cell Chem. Biol. 26 (2019) 1187–1194, https://doi.org/10.1016/j.chembiol.2019.05.003.
[34] J.C. Palomino, A. Martin, M. Camacho, H. Guerra, J. Swings, F. Portaels, Resazurin microtiter assay plate: simple and inexpensive method for detection of drug resistance in Mycobacterium tuberculosis, Antimicrob. Agents Chemother. 46 (2002) 2720–2722, https://doi.org/10.1128/AAC.46.8.2720-2722.2002.
[35] K. Billingsley, S.L. Buchwald, Highly efficient monophosphine-based catalyst for the palladium-catalyzed suzukimiyaura reaction of heteroaryl halides and heteroaryl boronic acids and esters, J. Am. Chem. Soc. 129 (2007) 3358–3366, https://doi.org/10.1021/ja068577p.
[36] B.L. Bray, P.H. Mathies, R. Naef, D.R. Solas, T.T. Tidwell, D.R. Artis, J.M. Muchowski, N-(triisopropylsilyl)pyrrole. a progenitor "par excellence" of 3-substituted pyrroles, J. Org. Chem. 55 (1990) 6317–6328, https://doi.org/10.1021/jo00313a019.
[37] A. Álvarez, A. Guzmán, A. Ruiz, E. Velarde, J.M. Muchowski, Synthesis of 3-arylpyrroles and 3-pyrrolylacetylenes by palladium catalyzed coupling reactions, J. Org. Chem. 57 (1992) 1653–1656, https://doi.org/10.1021/jo00032a011.
[38] H. Luo, Y. Lin, F. Gao, C.-T. Zhang, R. Zhang, DEG 10, an update of the Database of Essential Genes that includes both protein-coding genes and non-coding genomic elements, Nucleic Acids Res. 42 (2014) D574–D580, https://doi.org/10.1093/nar/gkt1131.
[39] DEG database. http://www.essentialgene.org/, 2021. (Accessed 23 December 2021).
[40] E. Adams, L. Frank, Metabolism of proline and the hydroxyprolines, Annu. Rev. Biochem. 49 (1980) 1005–1061, https://doi.org/10.1146/annurev.bi.49.070180.005041.
[41] D.J. Hayzer, T. Leisinger, The gene-enzyme relationships of proline biosynthesis in Escherichia coli, J. Gen. Microbiol. 118 (1980) 287–293, https://doi.org/10.1099/00221287-118-2-287.
[42] I. Massarelli, G. Forlani, E. Ricca, M. De Felice, Enhanced and feedback-resistant gamma-glutamyl kinase activity of an Escherichia coli transformant carrying a mutated proB gene of Streptococcus thermophilus, FEMS Microbiol. Lett. 182 (2000) 143–147, https://doi.org/10.1111/j.1574-6968.2000.tb08888.x.
[43] L.T. Smith, Characterization of a γ-glutamyl kinase from Escherichia coli that confers proline overproduction and osmotic tolerance, J. Bacteriol. 164 (1985) 1088–1093, https://doi.org/10.1128/jb.164.3.1088-1093.1985.
[44] T. Fujita, A. Maggio, M. Garcia-Rios, C. Stauffacher, R.A. Bressan, L.N. Csonka, Identification of regions of the tomato γ-glutamyl kinase that are involved in allosteric regulation by proline, J. Biol. Chem. 278 (2003) 14203–14210, https://doi.org/10.1074/jbc.M212177200.
[45] C. Marco-Marín, F. Gil-Ortíz, I. Pérez-Arellano, J. Cervera, I. Fita, V. Rubio, A novel two-domain architecture within the amino acid kinase enzyme family revealed by the crystal structure of Escherichia coli glutamate 5-kinase, J. Mol. Biol. 367 (2007) 1431–1446, https://doi.org/10.1016/j.jmb.2007.01.073.
[46] A. Fiser, A. Sali, ModLoop: automated modeling of loops in protein structures, Bioinformatics 19 (2003) 2500–2501, https://doi.org/10.1093/bioinformatics/btg362.
[47] L.A. Kelley, S. Mezulis, C.M. Yates, M.N. Wass, M.J. Sternberg, The Phyre2 web portal for protein modeling, prediction and analysis, Nat. Protoc. 10 (2015) 845–858, https://doi.org/10.1038/nprot.2015.053.
[48] G. Jones, P. Willett, R.C. Glen, A.R. Leach, R. Taylor, Development and validation of a genetic algorithm for flexible docking, J. Mol. Biol. 267 (1997) 727–748, https://doi.org/10.1006/jmbi.1996.0897.
[49] X. Liu, D. Shi, S. Zhou, H. Liu, H. Liu, X. Yao, Molecular dynamics simulations and novel drug discovery, Expet Opin. Drug Discov. 13 (2018) 23–37, https://doi.org/10.1080/17460441.2018.1403419.
[50] P. Śledź, A. Caflisch, Protein structure-based drug design: from docking to molecular dynamics, Curr. Opin. Struct. Biol. 48 (2018) 93–102, https://doi.org/10.1016/j.sbi.2017.10.010.
[51] J. Gorman, L. Shapiro, S.K. Burley, Crystal structure of glutamate 5-kinase from Campylobacter jejuni. https://doi.org/10.2210/pdb2AKO/pdb, 2022.
[52] M. Li, Y. Wang, R. Banerjee, F. Marinelli, S. Silberberg, J.D. Faraldo-Gómez, M. Hattori, K.J. Swartz, Molecular mechanisms of human P2X3 receptor channel activation and modulation by divalent cation bound ATP, Elife 8 (2019), e47060, https://doi.org/10.7554/eLife.47060.
[53] D.M. Pinkas, J.C. Bufton, J.A. Newman, J. Kopec, O. Borkowska, R. Chalk, N.A. Burgess-Brown, F. von Delft, C.H. Arrowsmith, A.M. Edwards, C. Bountra, A. Bullock, Crystal structure of WNK3 kinase domain in a diphosphorylated state and in complex with AMP-PNP/Mg2+. https://doi.org/10.2210/pdb5o26/pdb, 2022.
[54] I. Pérez-Arellano, F. Gil-Ortiz, J. Cervera, V. Rubio, Glutamate-5-kinase from Escherichia coli: gene cloning, overexpression, purification and crystallization of the recombinant enzyme and preliminary X-ray studies, Acta Crystallogr. D60 (2004) 2091–2094, https://doi.org/10.1107/S0907444904023972.
[55] I. Pérez-Arellano, V. Rubio, J. Cervera, Mapping active site residues in glutamate-5-kinase. The substrate glutamate and the feed-back inhibitor proline bind at overlapping sites, FEBS Lett. 580 (2006) 6247–6253, https://doi.org/10.1016/j.febslet.2006.10.031.
[56] J.C. Gordon, J.B. Myers, T. Folta, V. Shoja, L.S. Heath, A. Onufriev, H++: a server for estimating pKas and adding missing hydrogens to macromolecules, Nucleic Acids Res. 33 (2005) W368–W371, https://doi.org/10.1093/nar/gki464. Web Server issue).
[57] J.C. Vázquez-Ucha, D. Rodríguez, C. Lasarte-Monterrubio, E. Lence, J. Arca-Suarez, M. Maneiro, E. Gato, A. Perez, M. Martínez-Guitián, C. Juan, A. Oliver, G. Bou, C. González-Bello, A. Beceiro, A. 6-Halopyridylmethylidene penicillin-based sulfones efficiently inactivate the natural resistance of Pseudomonas aeruginosa to β-lactam antibiotics, J. Med. Chem. 64 (2021) 6310–6328, https://doi.org/10.1021/acs.jmedchem.1c00369.
[58] D.R. Roe, T.E. Cheatham, PTRAJ and CPPTRAJ: Software for processing and analysis of molecular dynamics trajectory data, J. Chem. Theor. Comput. 9 (2013) 3084–3095, https://doi.org/10.1021/ct400341p.
[59] W.L. DeLano, The PyMOL Molecular Graphics System, DeLano Scientific LLC, Palo Alto, CA, 2008. http://www.pymol.org/. (Accessed 1 July 2021), 2021.
[60] M.J. Frisch, G.W. Trucks, H.B. Schlegel, G.E. Scuseria, M.A. Robb, J.R. Cheeseman, G. Scalmani, V. Barone, B. Mennucci, G.A. Petersson, H. Nakatsuji, M. Caricato, X. Li, H.P. Hratchian, A.F. Izmaylov, J. Bloino, G. Zheng, J.L. Sonnenberg, M. Hada, M. Ehara, K. Toyota, R. Fukuda, J. Hasegawa, M. Ishida, T. Nakajima, Y. Honda, O. Kitao, H. Nakai, T. Vreven, J.A. Montgomery Jr., J.E. Peralta, F. Ogliaro, M. Bearpark, J.J. Heyd, E. Brothers, K.N. Kudin, V.N. Staroverov, R. Kobayashi, J. Normand, K. Raghavachari, A. Rendell, J.C. Burant, S.S. Iyengar, J. Tomasi, M. Cossi, N. Rega, J.M. Millam, M. Klene, J.E. Knox, J.B. Cross, V. Bakken, C. Adamo, J. Jaramillo, R. Gomperts, R.E. Stratmann, O. Yazyev, A.J. Austin, R. Cammi, C. Pomelli, J.W. Ochterski, R.L. Martin, K. Morokuma, V.G. Zakrzewski, G.A. Voth, P. Salvador, J.J. Dannenberg, S. Dapprich, A.D. Daniels, Ö. Farkas, J.B. Foresman, J.V. Ortiz, J. Cioslowski, D.J. Fox, Gaussian 09, Revision D.01, Gaussian, Inc., Wallingford CT, 2009.
[61] E. Vanquelef, S. Simon, G. Marquant, E. Garcia, G. Klimerak, J.C. Delepine, P. Cieplak, F.-Y. Dupradeau, R.E.D. Server, A Web service for deriving RESP and ESP charges and building force field libraries for new molecules and molecular fragment, Nucleic Acids Res. 39 (2011) W511–W517, https://doi.org/10.1093/nar/gkr288.
[62] RESP ESP charge derive home page. http://upjv.q4md-forcefieldtools.org/RED/, 2021. (Accessed 1 July 2021).
[63] F.-Y. Dupradeau, A. Pigache, T. Zaffran, C. Savineau, R. Lelong, N. Grivel, D. Lelong, W. Rosanski, P. Cieplak, The R.E.D. Tools: advances in RESP and ESP charge derivation and force field library building, Phys. Chem. Chem. Phys. 12 (2010) 7821–7839, https://doi.org/10.1039/c0cp00111b.
[64] W.D. Cornell, P. Cieplak, C.I. Bayly, I.R. Gould, K.M. Merz, D.M. Ferguson, D.C. Spellmeyer, T. Fox, J.W. Caldwell, P.A. Kollman, A second generation force field for the simulation of proteins, nucleic acids, and organic molecules, J. Am. Chem. Soc. 117 (1995) 5179–5197, https://doi.org/10.1021/ja00124a002.
[65] J. Wang, R.M. Wolf, J.W. Caldwell, P.A. Kollman, D.A. Case, Development and testing of a general amber force field, J. Comput. Chem. 25 (2004) 1157–1174, https://doi.org/10.1002/jcc.20035.
[66] J. Wang, W. Wang, P.A. Kollman, D.A. Case, Automatic atom type and bond type perception in molecular mechanical calculations, J. Mol. Graph. Model. 25 (2006) 247–260, https://doi.org/10.1016/j.jmgm.2005.12.005.
[67] R. Galindo-Murillo, D.R. Roe, T.E. Cheatham, Convergence and reproducibility in molecular dynamics simulations of the DNA duplex d(GCACGAACGAAC-GAACGC), Biochim. Biophys. Acta 1850 (2015) 1041–1058, https://doi.org/10.1016/j.bbagen.2014.09.007.
[68] B.R. Miller III, T.D. McGee Jr., J.M. Swails, N. Homeyer, H. Gohlke, A.E. Roitberg, MMPBSA.py: an efficient program for end-state free energy calculations, J. Chem. Theor. Comput. 8 (2012) 3314–3321, https://doi.org/10.1021/ct300418h.